



Flight Dynamics Modeling and Autopilot Design for Guided Projectiles via Linear Parameter-Varying Techniques

Gian Marco Vinco

► To cite this version:

Gian Marco Vinco. Flight Dynamics Modeling and Autopilot Design for Guided Projectiles via Linear Parameter-Varying Techniques. Automatic. Université Grenoble Alpes [2020-..], 2024. English. NNT : 2024GRALT011 . tel-04593695

HAL Id: tel-04593695

<https://theses.hal.science/tel-04593695v1>

Submitted on 30 May 2024

HAL is a multi-disciplinary open access archive for the deposit and dissemination of scientific research documents, whether they are published or not. The documents may come from teaching and research institutions in France or abroad, or from public or private research centers.

L'archive ouverte pluridisciplinaire **HAL**, est destinée au dépôt et à la diffusion de documents scientifiques de niveau recherche, publiés ou non, émanant des établissements d'enseignement et de recherche français ou étrangers, des laboratoires publics ou privés.

THÈSE

Pour obtenir le grade de

DOCTEUR DE L'UNIVERSITÉ GRENOBLE ALPES

École doctorale : EEATS - Electronique, Electrotechnique, Automatique, Traitement du Signal (EEATS)

Spécialité : Automatique - Productique

Unité de recherche : Grenoble Images Parole Signal Automatique

Approches linéaires à paramètres variants pour la modélisation de la dynamique du vol et la synthèse d'autopilotes des projectiles guidés

Flight Dynamics Modeling and Autopilot Design for Guided Projectiles via Linear Parameter-Varying Techniques

Présentée par :

Gian Marco VINCO

Direction de thèse :

Olivier SENAME

PROFESSEUR DES UNIVERSITES, Université Grenoble Alpes

Directeur de thèse

Guillaume STRUB

Institut franco-allemand de recherches de Saint-Louis (ISL)

Co-encadrant de thèse

Spilios THEODOULIS

Associate professor, Université de technologie de Delft

Co-encadrant de thèse

Rapporteurs :

Marco LOVERA

FULL PROFESSOR, École polytechnique de Milan

John ECONOMOU

FULL PROFESSOR, Université de Cranfield

Thèse soutenue publiquement le **2 février 2024**, devant le jury composé de :

John-Jairo MARTINEZ-MOLINA,

PROFESSEUR DES UNIVERSITES, GRENOBLE INP

Président

Olivier SENAME,

PROFESSEUR DES UNIVERSITES, GRENOBLE INP

Directeur de thèse

Marco LOVERA,

FULL PROFESSOR, École polytechnique de Milan

Rapporteur

John ECONOMOU,

FULL PROFESSOR, Université de Cranfield

Rapporteur

Charles POUSSOT-VASSAL,

DIRECTEUR DE RECHERCHE, ONERA

Examineur

Elmar WALLNER,

SENIOR SCIENTIST, MBDA Deutschland GmbH

Examineur

Invités :

Guillaume STRUB

CHARGE DE RECHERCHE, Institut franco-allemand de recherches de Saint-Louis

Spilios THEODOULIS

ASSOCIATE PROFESSOR, Université de technologie de Delft

Acknowledgments

This project has represented an incredible journey rich in achievements and difficulties. People who have played a significant role in the last three years of my life are too many to be mentioned, but I'll try to reach as many as I can.

There are not enough words to express my sincere gratitude to my supervisors Olivier Sename, Spilios Theodoulis, and Guillaume Strub for their guidance and support throughout the entire duration of the project. Besides the invaluable expertise and academic passion they transmitted to me as mentors, they have always encouraged and motivated me during the most challenging times of the project. Their patience and positive attitude have been the real key to facing any problems I encountered on the way. I will always be immensely grateful for the time and the kindness you have dedicated to me during these years.

An immense thanks go to my colleagues at GIPSA-lab and at ISL for all the laughs, the constructive discussions, and the coffee breaks we shared. Your support, your passion, and your energy have been an inspiring source of motivation and personal enrichment for my personal journey. I would particularly like to thank Ariel and Sofiane whom I started my Ph.D. with and whom I shared supervisors, conferences, struggles, and achievements. I have always found a good word, a cheer, and understanding from you. A chat in front of a beer might not solve LMIs (and believe me sometimes it does), but it is still refreshing.

I cannot forget my beloved flatmates Massimiliano, Nastja, Paolo, Konstantina and Benjamin. Together we shared broken washing machines, several tons of pizza and sushi, Batmaz threats, TV series, unexpected 16-km runs, ski trips, and a lot more. I have always thought that traveling was the best way to meet interesting people, but I wouldn't have expected to find someone like you guys on my way and share this much in such a short period of time.

To all the friends I met in Saint-Louis and Grenoble, for the ones back to Verona, and those spread across many other countries, thank you for sharing some of the happiest moments of these last years. I am still not sure where the next step of my journey will lead me, but I will always bring all the good memories I have with you wherever I'll be.

A special thanks go to my girlfriend Lauriane who has supported and endured me despite the stress of the last part of the project. You made everything easier and lighter, finding the right words or simply with a huge hug. Thank you for all your smiles and your sweetness.

Finally, I want to dedicate this work to my family who has been there since day one, always cheering and believing in me even when I didn't think I could do it. To all of you who were there waiting for me every time I was coming back home. Without you I would have never reached any of my achievements and, more importantly, I wouldn't be the person I am. You have always been an inexhaustible source of motivation. Thank you, I love you all.

“Aut viam inveniam aut faciam”

Hannibal Barca

*“Weren’t there times when everybody, or at least a few people, just panicked?
No, when bad things happened, we just calmly laid out all the options, and
failure was not one of them.
We never panicked, and we never gave up on finding a solution.”*

Apollo XIII

Contents

Résumé de Thèse	vii
Table of Acronyms	xxv
Nomenclature	xxvii
Introduction	1
List of Publications	13
 I Projectile Modeling Design: From the nonlinear to the LPV-based model formulation	 15
 1 Flight Dynamics Modeling	 17
1.1 Introduction	17
1.2 Flight Mechanics	19
1.3 Projectile Aerodynamic Characterization	32
1.4 6-DoF Simulator Environment	52
1.5 Concluding Remarks	57
 2 LPV Control-Oriented Modeling	 61
2.1 Introduction	61
2.2 LPV Framework	63
2.3 The State Transformation Approach	70
2.4 Polytopic Modeling Process	85
2.5 Concluding Remarks	95

II Projectile Autopilot Design: LPV-based robust controller design approaches for guided munitions	97
3 LPV Controller Design	99
3.1 Introduction	99
3.2 Fundamentals on LPV Control Design	101
3.3 Polytopic Controller Design	114
3.4 Grid-Based Controller Design	122
3.5 Concluding Remarks	133
4 Controller Performance and Robustness Assessment	135
4.1 Introduction	135
4.2 Background on Robustness Analysis	137
4.3 Controllers Robustness Analysis	147
4.4 Tracking Performance Simulations	155
4.5 Concluding Remarks	172
Conclusion and Perspectives	173
A Aerodynamic Analysis	177
A.1 Static Coefficients CFD Acquisitions	177
A.2 Multivariable Regression Model Derivation	180
A.3 Regression Models: Accuracy Comparison Results	183
B State Transformation Conditions	187
Bibliography	202

Résumé de Thèse

Contextualisation du Projet

Le développement des technologies sophistiquées de missiles et de munitions d'artillerie a toujours été synonyme de puissance, depuis leurs conceptions balistiques initiales non guidées. L'avènement des technologies de guidage avancées a encore renforcé leur utilisation en tant qu'armes conventionnelles, grâce à une précision accrue sur la cible. Les premières stratégies de guidage utilisaient des mesures radar ou optiques depuis le site de lancement, avec des commandes de contrôle radio ou laser transmises par un opérateur au sol. L'amélioration de la précision du guidage, notamment par l'utilisation de caméras de télévision et de faisceaux laser pour l'interception de la cible, a suscité un intérêt croissant pour le développement de munitions guidées. La conception des armes guidées repose sur trois fonctionnalités principales : le Guidage, la Navigation et le Contrôle (GNC). L'implémentation standard à double boucle GNC comprend une boucle interne rapide, qui met à jour les commandes de contrôle du pilote automatique en fonction des informations de navigation, et une boucle externe plus lente, qui ajuste les signaux de référence pour répondre aux exigences de la mission.

La dérivation d'une loi de contrôle efficace repose fortement sur l'exactitude du modèle choisi pour représenter la dynamique du système. La modélisation et la conception de contrôle ont toujours représenté des processus fastidieux à accomplir en raison de la grande non-linéarité caractérisant la dynamique de vol des missiles/projectiles et de la grande variété des paramètres opérationnels. Néanmoins, la complexité du modèle affecte la sélection de l'approche de contrôle la plus appropriée et éventuellement la charge numérique de la mise en œuvre du contrôleur. Dans ce contexte, une stratégie bien établie consiste à décomposer la tâche de contrôle globale en la conception de contrôleurs LTI locaux à chaque linéarisation locale de la dynamique non linéaire d'origine. L'ensemble résultant de contrôleurs LTI locaux peut être facilement mis en œuvre grâce à la définition d'une stratégie de planification dédiée, qui permet de sélectionner le contrôleur le plus approprié dans toutes les conditions de fonctionnement. La stratégie de planification la plus traditionnelle repose sur l'interpolation

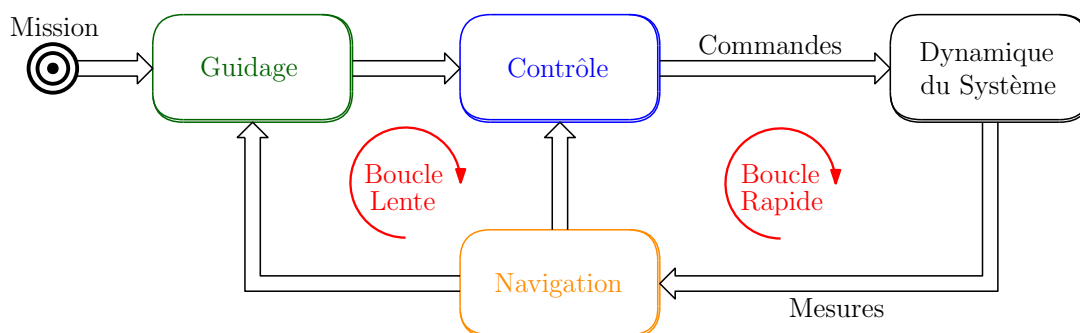


Figure 1 : Double boucle du système de guidage, navigation et contrôle (GNC).

linéaire des gains statiques des contrôleurs locaux, appelée planification de gain. Malgré une large gamme d'applications réussies, la conception de la planification de gain s'est avérée présenter des limitations de précision et de stabilité théoriques et pratiques pertinentes.

Ces dernières décennies, le cadre linéaire à paramètres variables (LPV) a émergé comme une alternative intéressante en modélisation et contrôle pour diverses applications aérospatiales. Contrairement à l'approche de linéarisation, la conception LPV vise directement la synthèse globale du contrôleur, assurant des propriétés de stabilité en boucle fermée à l'échelle globale. Les modèles LPV/quasi-LPV prennent en compte les variations temporelles d'un ensemble de paramètres sélectionnés, permettant une meilleure capture de la dynamique non linéaire du système. La synthèse du contrôleur LPV repose sur la formulation d'un problème d'optimisation dédié, réalisable soit en exploitant les caractéristiques des systèmes à affinité de paramètres, soit par une discrétisation de l'espace des paramètres à l'aide d'un processus de maillage. La première approche (polytopique) garantit une stabilité quadratique plus élevée, mais avec des performances plus conservatrices, tandis que la seconde (basée sur le maillage) offre des performances significatives avec une complexité de mise en œuvre plus élevée et des propriétés de stabilité globale réduites.

Dans ce contexte, le projet présenté propose l'analyse de la modélisation et de la conception de contrôle d'un nouveau concept de projectile guidé à longue portée (LRGP) étudié à l'Institut franco-allemand de recherche de Saint-Louis (ISL). Basé sur une architecture stabilisée par ailettes non rotatives de 155 mm, le projectile comprend quatre ailettes arrière axiales symétriques et deux canards avant pour les manœuvres de contrôle, configurés en 'X' comme illustré dans la Figure 2. L'objectif est d'améliorer la portée des obusiers standard sans recourir à des propulseurs supplémentaires ou des modifications du système de tir. La modélisation et la conception de contrôle sont étudiées dans le cadre LPV en raison de ses avantages et des applications limitées dans la littérature sur les technologies de munitions guidées.

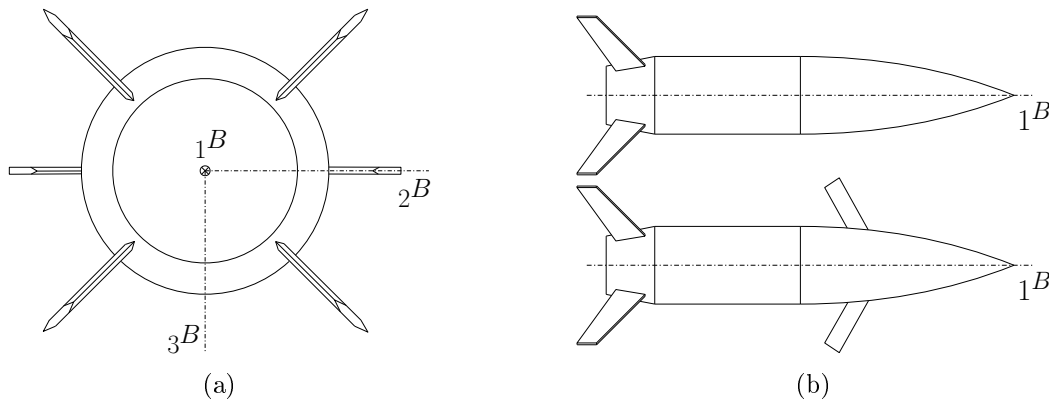


Figure 2 : Concept LRGP : (a) configuration ailerons-canards en "X" ; (b) configuration du projectile balistique (en haut) et du projectile planeur (en bas).

Chapitre 1 : Développement du Modèle de Projectile

Le processus de modélisation de la dynamique du système est crucial avant la conception du contrôleur. Une identification précise du comportement du système améliore la fiabilité du modèle mathématique et l'efficacité du contrôleur. Habituellement, des dynamiques de modèle simplifiées sont dérivées pour la conception du contrôleur, ne capturant que les caractéristiques les plus pertinentes pour les performances du contrôleur. Ensuite, un modèle détaillé est utilisé pour tester la conception du contrôleur dans un scénario de simulation plus réaliste. Pour le concept LRGP, la modélisation repose sur la formulation standard des équations différentielles non linéaires décrivant la dynamique inertielle du projectile. Des simulations de dynamique des fluides numériques (CFD) ont été réalisées pour caractériser l'aérodynamique du concept LRGP, ciblant les deux principales contributions aérodynamiques du projectile. Une première campagne a examiné les coefficients aérodynamiques générés par les contributions statiques de portance et de traînée du projectile, incluant l'effet des surfaces de contrôle à déflexion locale nulle. Le deuxième ensemble de données a étudié les contributions aérodynamiques supplémentaires générées par la déflexion locale des surfaces de contrôle.

Afin de fournir un modèle continu décrivant l'aérodynamique du projectile dans toutes les conditions de vol, les données CFD ont été traitées par le biais d'une analyse de régression précise. Un modèle polynomial à variable unique (PR) et un modèle multivariable (MR) ont été obtenus à partir de la régression des coefficients statiques. Le modèle PR est basé sur un ensemble réduit de données CFD, ciblant certaines configurations spécifiques et conditions de vol de l'aérodynamique du projectile. Le modèle MR, quant à lui, repose sur l'ensemble complet des données CFD acquises, fournissant une description aérodynamique globale qui couvre une gamme plus étendue de conditions de vol. Une régression polynomiale a également été réalisée sur l'ensemble de données CFD des surfaces de contrôle. Dans un souci de modélisation, les contributions aérodynamiques individuelles des surfaces de contrôle ont été formulées comme des effets globaux sur le taux de rotation du corps, influençant l'orientation du projectile. La formulation du contrôle reposait sur des hypothèses de superposition linéaire concernant la réponse aérodynamique du projectile. L'intervalle de confiance du modèle aérodynamique a été estimé pour une déviation totale : $\delta \in [-20, 20]$ deg.

À partir des résultats de modélisation, plusieurs modèles ont été élaborés pour représenter différentes caractéristiques de la dynamique du projectile. En fonction du niveau de précision et de complexité, chacun de ces modèles peut être utilisé à différentes étapes de la conception et de la validation de l'autopilote. Le premier modèle visait à représenter la dynamique de tangage du projectile, en incluant la dynamique de l'angle d'attaque (AoA), α , du taux de tangage, \dot{q} , le modèle aérodynamique statique PR, ainsi que les contributions aérodynamiques des surfaces de contrôle. Ce modèle a été utilisé ultérieurement pour la modélisation LPV et la conception de l'autopilote dédié au tangage. Le deuxième modèle reposait sur une description non linéaire 6-DoF de la dynamique translationnelle et d'attitude du projectile, en incluant le modèle aérodynamique MR complet ainsi que les contributions de contrôle aérodynamique correspondantes. Ce modèle a été implémenté dans un environnement de simulateur non linéaire 6-DoF pour évaluer les performances des contrôleurs.

Chapitre 2 : Dérivation du Modèle LPV

La modélisation orientée vers le contrôle consiste en une étape intermédiaire qui permet l'application de plusieurs approches de conception de contrôle aux dynamiques non linéaires générales d'un système. Le cadre linéaire à paramètres variables (LPV) permet une représentation plus générale et complète des dynamiques temporelles du système, exploitée à travers la sélection d'un ensemble de paramètres variables, $\boldsymbol{\rho}$. Plusieurs applications aérospatiales réussies ont été proposées ces dernières années, reformulant les dynamiques non linéaires standard du véhicule en un modèle LPV/quasi-LPV précis. La conversion peut être réalisée par l'emploi de différentes approches LPV telles que la substitution de fonctions, les techniques basées sur la vitesse et la transformation d'état.

La méthode de transformation d'état a été privilégiée pour développer un modèle LPV précis de la dynamique de tangage du projectile, offrant une transformation exacte entre le système non linéaire d'origine et le modèle LPV résultant. Ainsi, aucune approximation n'a été nécessaire dans la conception, ce qui a renforcé la capacité du modèle à représenter la dynamique d'origine. Le vecteur de paramètres variables choisi est $\boldsymbol{\rho} = [\alpha, V, h]$, où V représente la vitesse de l'air du projectile et h l'altitude. Pour appliquer le processus de transformation, une approximation aérodynamique spécifique a été développée, exprimant le coefficient de contrôle aérodynamique comme une fonction linéaire de la déflexion des canards, répondant ainsi aux exigences de l'approche de transformation d'état. De plus, la dynamique de l'intégrateur a été ajoutée à l'entrée du système pour compenser la configuration dépendante des paramètres d'entrée.

Le modèle quasi-LPV augmenté d'intégrateur de la dynamique de tangage du projectile, désigné par Σ_{GR} , a été utilisé pour la conception du contrôleur basé sur la grille LPV. Dans l'équation de sortie, les mesures du facteur de charge hors équilibre, $\eta_{z,dev}$, ont remplacé la déflexion de tangage des canards, δ_q . La matrice d'avance, \mathcal{D} , a été supposée nulle. L'exactitude du modèle quasi-LPV a été confirmée par simulation sur une plage de variation incluant $\alpha \in [0, 16]$ degrés, $V \in [160, 280]$ m/s, $h \in [1, 15]$ km.

Dans le but d'utiliser le modèle quasi-LPV pour la conception d'un contrôleur polytopique basé sur le LPV, une étape de modélisation supplémentaire a été nécessaire. En effet, le modèle quasi-LPV obtenu ne respectait pas la relation affine entre le modèle et les paramètres imposée par la formulation polytopique. Ainsi, une procédure d'approximation du modèle a été développée dans le but de reformuler le modèle quasi-LPV du projectile en un système polytopique. L'approximation reposait sur l'identification d'un nouvel ensemble de fonctions de planification, $\hat{\boldsymbol{\rho}}$, affines par rapport à la dynamique du système. Le processus d'approximation a abouti à la reformulation polytopique de la dynamique de tangage quasi-LPV du projectile, Σ_{PY} . Concernant l'équation de sortie, la matrice de sortie, \mathcal{C} , est constituée de la matrice identité, $I \in \mathbb{R}^{3 \times 3}$, en supposant une architecture de rétroaction d'état. La matrice d'avance, \mathcal{D} , est supposée nulle. Après avoir évalué l'exactitude du processus d'approximation, le domaine d'application original du modèle quasi-LPV a été cartographié dans le nouveau polytope convexe, $\hat{\Theta}$, défini par les fonctions de planification : $\hat{\rho}_1(V, h) \in [0.4, 2.9] \times 10^4$, $\hat{\rho}_2(\alpha, V, h) \in [0.05, 0.55]$, et $\hat{\rho}_3(\alpha, V, h) \in [-1, 4.1]$.

Chapitre 3 : Conception de l'Autopilote LPV de Tangage

La synthèse des contrôleurs LPV repose sur la résolution de problèmes d'optimisation convexes formulés sous forme d'inégalités matricielles linéaires (LMIs). En imposant une relation affine entre le modèle et les paramètres, l'optimisation peut être résolue dans un sous-espace convexe (polytope) défini par les plages de variation du paramètre. En exploitant la variation linéaire du paramètre, la conception garantit des garanties de stabilité dans tout le polytope. Une autre approche consiste à discrétiser l'espace de variation des paramètres en un ensemble fini de conditions de conception (gridding), tout en tenant compte du taux de variation de chaque paramètre pour améliorer les performances du contrôleur. Ces approches ont été utilisées pour synthétiser un pilote automatique LPV pour la dynamique de tangage du projectile.

En ce qui concerne l'approche polytopique, les conditions du problème d'optimisation LMIs doivent être satisfaites uniquement aux sommets de l'espace convexe défini par les plages de variation des fonctions de planification. Les principaux avantages de cette approche reposent sur le nombre réduit de conditions à satisfaire simultanément et sur les garanties accrues de stabilité quadratique dans tout le domaine couvert par le polytope convexe. Le principal inconvénient réside dans le conservatisme qui affecte le processus d'optimisation, car la solution est basée sur une fonction de Lyapunov indépendante des paramètres. Afin d'améliorer les performances de l'optimisation, une analyse dédiée est développée pour optimiser la dimension du polytope, en négligeant toutes les conditions opérationnelles qui n'appartiennent pas à l'enveloppe de vol du projectile. L'analyse a permis de définir un polytope de dimensions réduites, $\hat{\Theta}_R$, en ajustant les plages de variation des fonctions de planification comme suit : $\hat{\rho}_1 \in [0.4, 2] \times 10^4$, $\hat{\rho}_2 \in [0.05, 0.35]$, et $\hat{\rho}_3 \in [-1, 2]$.

La conception du contrôleur polytopique résultant était basée sur le schéma de la Figure 3, en supposant le critère d'optimisation \mathcal{H}_∞ . La conception vise à améliorer la robustesse du contrôleur, en tenant compte d'un ensemble de sources internes et externes de perturbation (d_i , d_o), et de la capacité à suivre un signal de guidage de référence, r , en imposant un modèle de référence, f_{ref} , et un ensemble de filtres de pondération de performance, (W_r , W_e , W_u , Wd_i , Wd_o). La dynamique des actionneurs, T_{act} , est également incluse dans la conception du contrôleur.

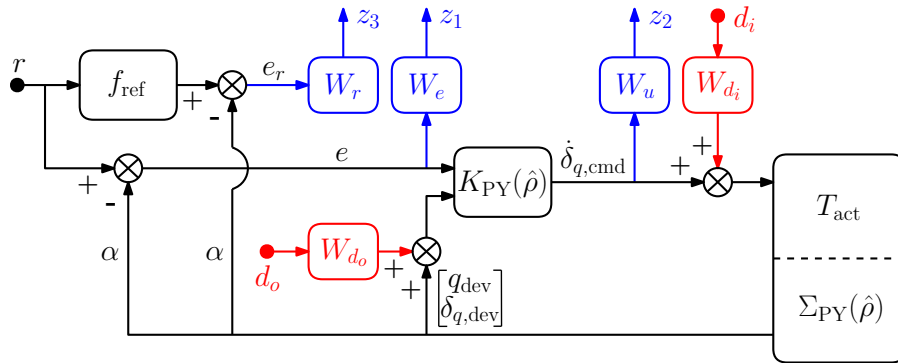


Figure 3 : Architecture du schéma de conception polytopique.

La deuxième approche repose sur la discrétisation (gridding) de l'espace de variation des variables de planification en une grille finie de conditions de vol. L'optimisation LMI définissant la synthèse du contrôleur est calculée à chacun des points de conception sélectionnés. En conséquence, la complexité computationnelle affectant l'optimisation dépend fortement de la définition de la grille. Cependant, la solution du problème LMI est basée sur des fonctions de Lyapunov dépendantes des paramètres, ce qui offre de meilleures performances d'optimisation. Pour limiter la complexité computationnelle, une analyse exhaustive de l'enveloppe de vol discrétisée a ciblé les propriétés de stabilité du système et les performances de trajectoire souhaitées. L'analyse visait à trouver une dimension de grille optimale en équilibrant la complexité computationnelle et les garanties de stabilité. De plus, la paramétrisation des fonctions de Lyapunov a été étudiée pour modéliser la dépendance des fonctions sur chaque variable de planification. Les résultats de l'analyse fournissent les plages de variations discrétisées suivantes : $\alpha_{\text{grid}} = [1, 5, 8, 13]$ degrés, $V_{\text{grid}} = [180, 200, 240, 270]$ m/s, et $h_{\text{grid}} = [3, 6, 9, 12, 14.5]$ km, tandis que les fonctions de Lyapunov ont été formulées comme suit :

$$X(\rho) = Y(\rho) = X_0 + X_{\alpha,1} \sin \alpha + X_{\alpha,2} \cos \alpha + X_V V + X_h h.$$

La conception du contrôleur LPV/ \mathcal{H}_∞ a été basée sur le schéma de la Figure 4 et a été calculée sur l'espace de grille résultant, Ξ , composé de $n_g = 80$ points de vol. Les taux de variation de chaque variable de planification ont été définis comme suit : $\dot{\alpha}_{\text{grid}} \in [-30, 30]$ deg/s, $\dot{V}_{\text{grid}} = [-50, 50]$ m/s², et $\dot{h}_{\text{grid}} = [-100, 100]$ m/s.

La conception polytopique est basée sur une approximation supplémentaire de modélisation, introduisant des sources indésirables d'incertitudes. Cependant, l'approche polytopique garantit des propriétés de stabilité robustes supérieures dans tout l'espace convexe. En ce qui concerne la conception basée sur la grille, des garanties de stabilité robustes ne sont fournies qu'à proximité des points de conception. D'autre part, les performances d'optimisation attendues étaient confirmées à la fois par les résultats de γ_∞ inférieurs et par l'effort de commande réduit requis pour les actionneurs. Du point de vue de la complexité, la synthèse du contrôleur était basée sur la sélection de plusieurs paramètres de réglage (n_g, \mathbf{f}_B), nécessitant le développement d'une analyse dédiée chronophage. Enfin, la mise en œuvre du contrôleur basé sur la grille, K_{GR} , repose sur l'interpolation de 80 réalisations locales LTI, comparé aux 8 réalisations locales LTI requises par le contrôleur polytopique, K_{PY} .

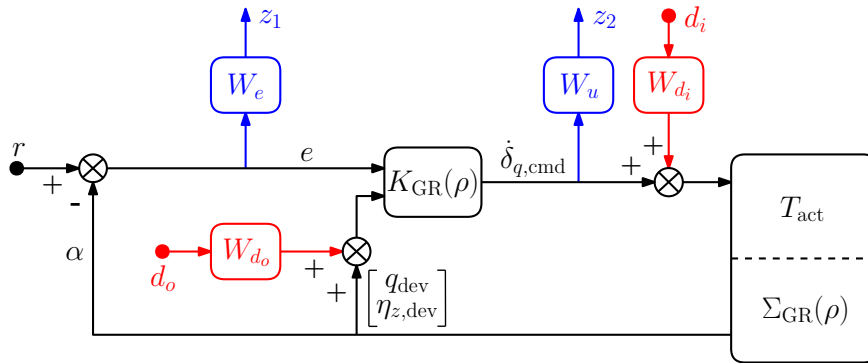


Figure 4 : Architecture du schéma de conception basé sur la grille.

Chapitre 4 : Évaluation des Performances

Les procédures standards de conception de contrôle visent la stabilité nominale (NS) et les performances (NP) du système en boucle fermée. Toutefois, les perturbations possibles peuvent dévier la dynamique du système de ses conditions nominales. La performance des contrôleurs polytopique, K_{PY} , et basé sur la grille, K_{GR} , a été examinée face à diverses perturbations et incertitudes du modèle. Une première analyse de robustesse a évalué les marges de stabilité des fonctions de transfert entrée/sortie pour chaque système. Comme les modèles quasi-LPV et polytopiques sont des systèmes à entrée unique et à sortie multiple, le calcul des marges de disque est préféré aux définitions standard des marges de gain et de phase. Les résultats montrent de larges marges de sortie pour la dynamique des première et troisième voies ($\dot{\alpha}$ et $\dot{\delta}_{q,dev}$), mais des faiblesses potentielles sont apparues pour la deuxième voie (\dot{q}).

Les marges de stabilité fournissent des conditions nécessaires mais pas suffisantes pour évaluer la robustesse du système et peuvent conduire à une analyse très conservatrice. Ainsi, les performances des contrôleurs ont été testées plus avant à travers une analyse de sensibilité μ , visant la robustesse par rapport aux incertitudes paramétriques structurées du système. Un ensemble de paramètres a été sélectionné en fonction de l'effet de leur variation sur la stabilité de la dynamique du système. L'ensemble d'incertitudes comprend une sélection de paramètres aérodynamiques, chacun associé à une plage de tolérance estimée (exprimée en pourcentage d'incertitude). Cependant, en raison de la complexité excessive de la formulation numérique, les incertitudes paramétriques individuelles ont été modélisées comme des perturbations globales affectant chaque entrée de la représentation de l'espace d'état du système. L'analyse μ réalisée sur l'ensemble dédié d'incertitudes a révélé des propriétés de stabilité robuste et de performance robuste satisfaisantes des systèmes en boucle fermée polytopique et basé sur la grille par rapport aux incertitudes paramétriques. Le pourcentage d'incertitude du système que le contrôleur polytopique peut gérer est plus élevé par rapport au contrôleur basé sur la grille, en cohérence avec les garanties théoriques de stabilité fournies par la synthèse polytopique.

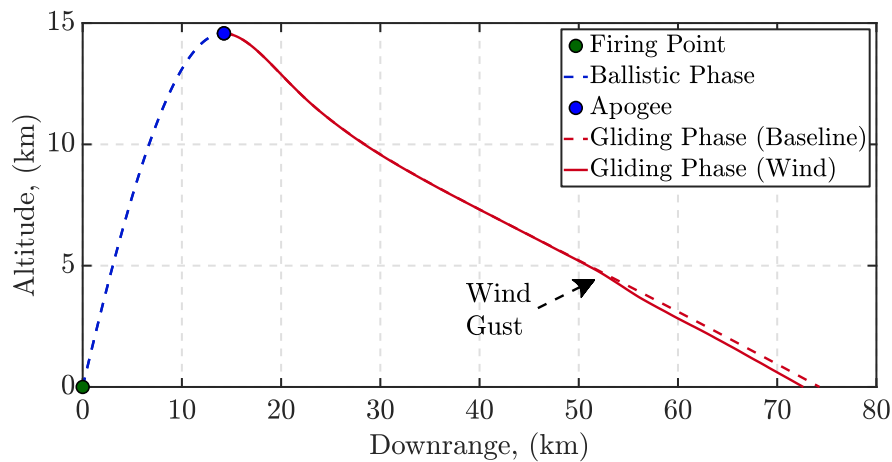


Figure 5: Comparaison des simulations : performances de la trajectoire.

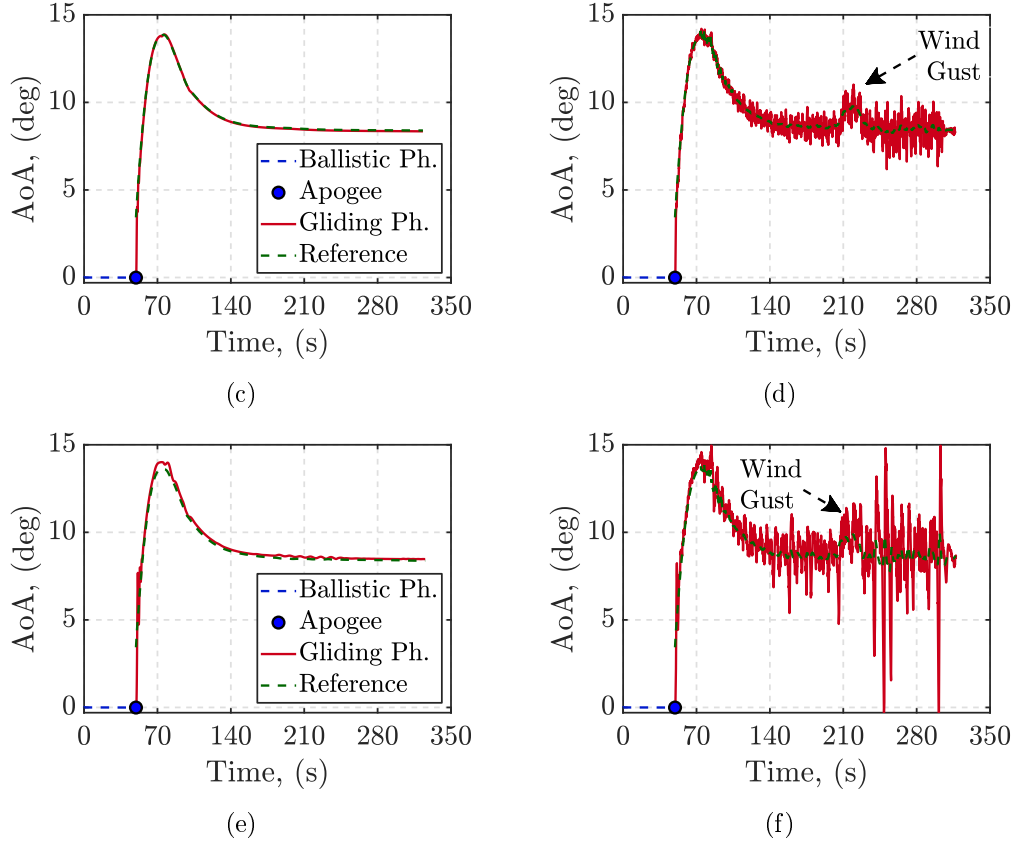


Figure 6: Trajectoires nominales et perturbées respectivement liées aux : (a)-(b) contrôleur polytopique ; (c)-(d) contrôleur basé sur la grille.

Enfin, les performances des contrôleurs ont été testées par rapport à l'effet des perturbations variant dans le temps. Une première série de simulations de suivi de trajectoire nominale a été réalisée en mettant en œuvre les contrôleurs dans un environnement de simulateur non linéaire 6-DoF. Les simulations ont permis d'identifier la vitesse de tir et l'angle d'élévation optimaux (939 m/s, 60 deg). Dans un deuxième temps, des perturbations dues au vent ont été incluses dans les scénarios de simulation sous forme de turbulences continues et de profils de vitesse de rafales de vent discrètes. La comparaison des trajectoires dans la Figure 5 montre comment les perturbations dues au vent affectent la capacité de portée du projectile en réduisant légèrement la distance maximale atteignable. De plus, les résultats de la Figure 6 confirment la robustesse des contrôleurs polytopique et basé sur la grille dans la gestion des oscillations de signaux importantes générées par la turbulence du vent. Malgré les oscillations, les systèmes parviennent à suivre avec succès le signal de AoA de guidage de référence sur toute la trajectoire. En ce qui concerne le contrôleur polytopique, les trajectoires des fonctions de planification perturbées se situent dans l'espace convexe utilisé lors de la synthèse du contrôleur, assurant ainsi la stabilité du système en boucle fermée même en présence de signaux de perturbation importants. Le contrôleur basé sur la grille a également réussi à préserver la stabilité du projectile sur toute la trajectoire, même si les paramètres de vol obtenus sont généralement affectés par des oscillations plus importantes autour de leurs valeurs nominales.

Conclusions et Perspectives

Cette thèse a étudié l'utilisation des techniques à paramètres linéaires variant (LPV) pour la modélisation et la conception de contrôle d'un nouveau concept de projectile guidé à longue portée (LRGP). Le développement d'une munition à portée étendue vise à combler l'écart technologique entre les projectiles balistiques/guidés lancés par canon standard et les applications de missiles à propulsion par fusée plus sophistiquées. Une contribution importante réside dans la caractérisation de la dynamique de vol/aérodynamique du nouveau concept de projectile et dans la proposition d'une procédure complète dédiée à la reformulation du modèle LPV. De plus, l'utilisation réussie de différentes approches de conception de contrôle basées sur LPV (polytopique, basée sur grille) a confirmé les avantages fournis par le cadre LPV pour ces technologies spécifiques, malgré la quantité limitée d'applications proposées dans la littérature.

Les résultats obtenus à travers les processus de modélisation LPV et de conception de contrôle suggèrent également plusieurs points d'amélioration possibles :

- ❖ **Régression Aérodynamique** : Le modèle aérodynamique pourrait être davantage développé en exploitant la dépendance des coefficients aérodynamiques par rapport à la variation de Mach.
- ❖ **Variables de Référence** : Le choix de l'angle d'attaque aérodynamique (AoA) comme variable de planification représente un choix assez inhabituel car des mesures précises nécessitent une instrumentation dédiée. La reformulation du modèle de vol du projectile en termes de dynamique d'accélération pourrait simplifier le processus de mise en œuvre.
- ❖ **Approche de Modélisation LPV** : Des techniques de modélisation alternatives pourraient être envisagées pour assouplir les contraintes imposées par l'approche de transformation d'état.
- ❖ **Définition du Polytope** : Une reformulation de la forme du polytope pourrait améliorer les performances de la conception du contrôle. Cela pourrait être réalisé en changeant de variables, en définissant le polytope autour de la trajectoire prévue du projectile.
- ❖ **Sélection de la Grille** : L'utilisation des fonctions MATLAB LPVTools pour la conception impose la définition d'une grille rectangulaire/cubique, ce qui peut entraîner l'inclusion de conditions de vol indésirables. Une reformulation appropriée du problème d'optimisation des LMI pourrait permettre de relâcher les contraintes de forme imposées par LPVTools.
- ❖ **Contrôleur Latéral** : La modélisation LPV et la conception de contrôle pourraient être étendues pour tenir compte de la dynamique de roulis et de lacet du projectile, permettant la mise en œuvre d'une stratégie de vol complète de virage sur l'aile.

List of Figures

1	Guidance, Navigation, and Control (GNC) double-loop design.	5
2	Gain-scheduling: (a) flight envelope parametrization; (b) controller, K , linear interpolation.	7
1.1	Main reference frames and coordinate systems: (a) Earth frame, E , and Earth and local-level coordinates; (b) body frame, B , and body coordinates.	22
1.2	Wind coordinate systems: (a) Cartesian incidence angles convention; (b) polar aeroballistic angles convention.	24
1.3	Projectile's linear and angular velocities components projected w.r.t. the body coordinates.	27
1.4	LRGP concept: (a) 'X' fins-canards configuration; (b) ballistic (top) and glider (bottom) projectile's configuration.	30
1.5	LRGP flight strategy: range-enhancement gliding trajectory.	30
1.6	Canards local control deflection.	33
1.7	CFD static lateral coefficient dataset, C_{Y_S} : (a) $\phi' = 0$ deg; (b) $\phi' = 15$ deg; (c) $\phi' = 30$ deg; (d) $\phi' = 45$ deg; (e) $\phi' = 90$ deg.	35
1.8	CFD static pitching moment coefficient dataset, C_{m_S} : (a) $\phi' = 0$ deg; (b) $\phi' = 15$ deg; (c) $\phi' = 30$ deg; (d) $\phi' = 45$ deg; (e) $\phi' = 90$ deg.	36
1.9	CFD Lift-to-Drag Ratio dataset, LDR: (a) $\phi' = 0$ deg; (b) $\phi' = 15$ deg; (c) $\phi' = 30$ deg; (d) $\phi' = 45$ deg; (e) $\phi' = 90$ deg.	37
1.10	CFD control coefficient dataset: (a) longitudinal force, $C_{X_{\delta_r}}$; (b) vertical force, $C_{Z_{\delta_r}}$; (c) rolling moment, $C_{l_{\delta_r}}$; (d) pitching moment, $C_{m_{\delta_r}}$	38
1.11	R^2 and NRMSE regression results: (a)-(d) longitudinal force coefficient, C_{X_S} ; (b)-(e) vertical force coefficient, C_{Z_S} ; (c)-(f) pitching moment coefficient, C_{m_S}	41
1.12	R^2 and NRMSE regression results: (a)-(c) lateral force coefficient, C_{Y_S} ; (b)-(d) yawing moment coefficient, C_{n_S}	41
1.13	R^2 and NRMSE regression results: (a)-(d) longitudinal force coefficient, C_{X_S} ; (b)-(e) lateral force coefficient, C_{Y_S} ; (c)-(f) vertical force coefficient, C_{Z_S}	43
1.14	R^2 and NRMSE regression results: (a)-(c) pitching moment coefficient, C_{m_S} ; (b)-(d) yawing moment coefficient, C_{n_S}	43

1.15	$C_{Z_{\delta}}$ interpolation NRMSE comparison at different flight conditions: (a) $\phi' = 0$ deg; (b) $\phi' = 30$ deg; (c) $\phi' = 45$ deg.	46
1.16	$C_{Y_{\delta}}$ interpolation NRMSE comparison at different flight conditions: (a) $\phi' = 15$ deg; (b) $\phi' = 45$ deg; (c) $\phi' = 90$ deg.	46
1.17	R^2 and NRMSE regression results: (a)-(c) longitudinal force control coefficient, $C_{X_{\delta_r}}$; (b)-(d) vertical force control coefficient, $C_{Z_{\delta_r}}$	47
1.18	R^2 and NRMSE regression results: (a)-(c) rolling moment control coefficient, $C_{l_{\delta_r}}$; (b)-(d) pitching moment control coefficient, $C_{m_{\delta_r}}$	47
1.19	Virtual control deflections: (a) roll coefficients; (b) pitch coefficients.	48
1.20	$C_{X_{\delta_{\text{eff}}}}$ coefficient linearity error surfaces at different flight regimes: (a) $\mathcal{M} = 0.3$; (b) $\mathcal{M} = 0.7$; (c) $\mathcal{M} = 1$	49
1.21	$C_{Z_{\delta_q}}$ coefficient linearity error surfaces at different flight regimes: (a) $\mathcal{M} = 0.3$; (b) $\mathcal{M} = 0.7$; (c) $\mathcal{M} = 1$	50
1.22	$C_{l_{\delta_p}}$ coefficient linearity error surfaces at different flight regimes: (a) $\mathcal{M} = 0.3$; (b) $\mathcal{M} = 0.7$; (c) $\mathcal{M} = 1$	50
1.23	$C_{m_{\delta_q}}$ coefficient linearity error surfaces at different flight regimes: (a) $\mathcal{M} = 0.3$; (b) $\mathcal{M} = 0.7$; (c) $\mathcal{M} = 1$	50
1.24	Nonlinear simulator: complete software environment.	53
1.25	Nonlinear simulator: projectile airframe architecture.	54
1.26	Ballistic simulations: trajectory performance comparison.	55
1.27	Ballistic simulations: (a) AoA trajectories; (b) Mach trajectories; (c) pitch angle trajectories; (d) pitch rate trajectories; (e) pitching moment trajectories.	56
2.1	Classification diagram of dynamical systems.	63
2.2	2D polytope representation.	66
2.3	$C_{Z_{\delta_q}}$ approximation errors: (a) e_{PR} related to the TA approach; (b) e_{PR} related to the LR approach; (c) e_{CFD} related to the TA approach; (d) e_{CFD} related to the LR approach.	76
2.4	$C_{m_{\delta_q}}$ approximation errors: (a) e_{PR} related to the TA approach; (b) e_{PR} related to the LR approach; (c) e_{CFD} related to the TA approach; (d) e_{CFD} related to the LR approach.	77
2.5	Trimming functions analysis: (a)-(b)-(c) pitch rate curves at $h = [1, 7, 15]$ km, respectively; (d)-(e)-(f) pitch deflection curves at $h = [1, 7, 15]$ km, respectively.	79

2.6	Trimming functions partial derivatives analysis: (a)-(b)-(c) pitch rate curves at $h = [1, 7, 15]$ km, respectively; (d)-(e)-(f) pitch deflection curves at $h = [1, 7, 15]$ km, respectively.	80
2.7	Simulation scheme: quasi-LPV model assessment.	82
2.8	Simulation curves comparison: (a) input perturbations; (b) angle-of-attack; (c) off-equilibrium pitch rate; (d) off-equilibrium pitch deflections.	83
2.9	Simulation curves comparison: (a) equilibrium pitch rate; (b) equilibrium pitch deflection; (c) total canards deflection.	84
2.10	Polytopic model approximation scheme.	86
2.11	Approximation analysis: (a) $\tilde{\rho}_1$ at $\alpha = 4$ deg; (b) $\tilde{\rho}_1$ at $\alpha = 12$ deg.	88
2.12	Approximation analysis: (a) NRMSE of $\tilde{\rho}_2$; (b) NRMSE of $\tilde{\rho}_5$; (c) NRMSE of $\tilde{\rho}_6$	89
2.13	Approximation analysis: (a)-(b) $\tilde{\rho}_3$ variation at $\alpha = 4$ deg, and $\alpha = 12$ deg, respectively; (c)-(d) $\tilde{\rho}_4$ variation at $\alpha = 4$ deg, and $\alpha = 12$ deg, respectively.	91
2.14	Pole-zero maps: (a) (V, h) variation at $\alpha = 12$ deg; (b) stable/unstable α conditions.	92
2.15	Flight points selection: (a) $V - h$ trajectory constraints; (b) (α, V, h) 3D subspace.	93
2.16	Polytope identification: (a) $\hat{\rho}_1$ - $\hat{\rho}_2$ subspace; (b) $\hat{\rho}_1$ - $\hat{\rho}_3$ subspace; (c) $\hat{\rho}_2$ - $\hat{\rho}_3$ subspace; (d) $(\hat{\rho}_1, \hat{\rho}_2, \hat{\rho}_3)$ 3D polytope.	94
3.1	Polytopic design scheme architecture.	115
3.2	General polytopic control scheme configuration.	115
3.3	Dependence on the altitude: (a) $\hat{\rho}_1$ - $\hat{\rho}_2$; (b) $\hat{\rho}_1$ - $\hat{\rho}_3$; (c) $\hat{\rho}_2$ - $\hat{\rho}_3$; (d) 3D space.	117
3.4	Polytope's 3D dimensions dependence: (a) airspeed; (b) AoA.	117
3.5	Polytope's dimensions dependence on the airspeed and AoA variations: (a)-(b) $\hat{\rho}_1$ - $\hat{\rho}_2$, respectively; (c)-(d) $\hat{\rho}_1$ - $\hat{\rho}_3$, respectively; (e)-(f) $\hat{\rho}_2$ - $\hat{\rho}_3$, respectively.	118
3.6	Reduced polytope $\hat{\Theta}_R$: (a) $\hat{\rho}_1$ - $\hat{\rho}_2$; (b) $\hat{\rho}_1$ - $\hat{\rho}_3$; (c) $\hat{\rho}_2$ - $\hat{\rho}_3$; (d) 3D space.	119
3.7	Polytopic design results: (a) Sensitivity functions; (b) Complementary Sensitivity functions.	120
3.8	Polytopic design results: (a) Plant Sensitivity functions; (b) Controller Sensitivity functions.	121

3.9	Grid-based design scheme architecture.	123
3.10	General grid-based control scheme configuration.	123
3.11	Dynamics dependence on the airspeed and altitude variations at: (a)-(b) $\alpha = 5$ deg, respectively; (c)-(d) $\alpha = 9$, respectively; (e)-(f) $\alpha = 13$ deg, respectively.	125
3.12	3D discretized system's stability envelope.	126
3.13	Reduced stability envelope based on trajectory considerations.	127
3.14	Performance level and computational time dependence on the grid points and basis functions selections: (a)-(b) AoA analysis, respectively; (c)-(d) airspeed analysis, respectively; (e)-(f) altitude analysis, respectively.	130
3.15	Grid-based design results: (a) Sensitivity functions; (b) Complementary Sensitivity functions; (c) Plant Sensitivity functions; (d) Controller Sensitivity functions.	132
4.1	Uncertainty representations: (a) additive; (b) output multiplicative.	138
4.2	LFT uncertain plant representations.	139
4.3	Stability margins analysis: (a) nominal open-loop transfer function; (b) Nyquist domain interpretation.	140
4.4	Loop-at-a-time disk margins computation scheme.	143
4.5	Robustness analysis schemes: (a) generalized uncertain control configuration; (b) standard $N\Delta$ structure; (b) standard $M\Delta$ closed-loop structure.	144
4.6	Augmented $N\hat{\Delta}$ structure for RP assessment.	145
4.7	Analysis schemes: (a) input disturbance; (b) output disturbance.	147
4.8	Input DKM: (a)-(c) polytopic/ grid-based Nyquist exclusion region, respectively; (b)-(d) polytopic/grid-based mutual GM/PM variation, respectively.	148
4.9	Polytopic output DKM Nyquist exclusion region and mutual GM/PM variation related to the: (a)-(b) α channel, respectively; (c)-(d) q_{dev} channel, respectively; (e)-(f) $\delta_{q,\text{dev}}$ channel, respectively.	150
4.10	Grid-based output DKM Nyquist exclusion region and mutual GM/PM variation related to the: (a)-(b) α channel, respectively; (c)-(d) q_{dev} channel, respectively; (e)-(f) $\eta_{z,\text{dev}}$ channel, respectively.	151
4.11	Polytopic closed-loop $M\Delta$ structure.	152
4.12	Polytopic system RS analysis results.	153

4.13	Grid-based system RS analysis results.	153
4.14	Polytopic system RP analysis results.	154
4.15	Grid-based system RP analysis results.	154
4.16	Nonlinear simulation implementation scheme.	155
4.17	K_{PY} and K_{GR} baseline simulations: trajectory performance comparison.	157
4.18	K_{PY} and K_{GR} baseline simulations: (a)-(b) V - h relation trajectories, respectively; (c)-(d) AoA trajectories, respectively; (e)-(f) canards total pitch deflection trajectories, respectively.	158
4.19	K_{PY} baseline simulations: (a) $\hat{\rho}_1$ trajectories; (b) $\hat{\rho}_2$ trajectories; (c) $\hat{\rho}_3$ trajectories; (d) 3D scheduling functions trajectories.	159
4.20	K_{GR} baseline simulations: 3D scheduling variables trajectories.	160
4.21	Wind velocity profile: (a) longitudinal; (b) vertical.	161
4.22	Polytopic simulations: trajectory performance.	162
4.23	Polytopic simulations: (a)-(b) AoA nominal and perturbed trajectories, respectively; (c)-(d) pitch rate nominal and perturbed trajectories, respectively; (e)-(f) pitch angle nominal and perturbed trajectories, respectively.	163
4.24	Polytopic simulations: (a)-(b) Mach nominal and perturbed trajectories, respectively; (c)-(d) V - h relation nominal and perturbed trajectories, respectively; (e)-(f) canards total pitch deflection nominal and perturbed trajectories, respectively.	164
4.25	Polytopic simulations: (a)-(b) $\hat{\rho}_1$ nominal and perturbed trajectories, respectively; (c)-(d) $\hat{\rho}_2$ nominal and perturbed trajectories, respectively; (e)-(f) $\hat{\rho}_3$ nominal and perturbed trajectories, respectively.	165
4.26	Polytopic simulations: (a) 3D nominal scheduling functions trajectories; (b) 3D perturbed scheduling functions trajectories.	166
4.27	Polytopic simulations: (a) 3D nominal interpolation functions trajectories; (b) 3D perturbed interpolation functions trajectories.	166
4.28	Grid-based simulations: trajectory performance.	167
4.29	Grid-based simulations: (a)-(b) AoA nominal and perturbed trajectories, respectively; (c)-(d) pitch rate nominal and perturbed trajectories, respectively; (e)-(f) pitch angle nominal and perturbed trajectories, respectively.	168

4.30	Grid-based simulations: (a)-(b) Mach nominal and perturbed trajectories, respectively; (c)-(d) V - h relation nominal and perturbed trajectories, respectively; (e)-(f) canards total pitch deflection nominal and perturbed trajectories, respectively.	169
4.31	Grid-based simulations: (a)-(b) AoA variation rate nominal and perturbed trajectories, respectively; (c)-(d) airspeed variation rate nominal and perturbed trajectories, respectively; (e)-(f) altitude variation rate nominal and perturbed trajectories, respectively.	170
4.32	Grid-based nominal simulation: 3D scheduling variables trajectory.	171
4.33	Grid-based perturbed simulation: 3D scheduling variables trajectory.	171
A.1	CFD static longitudinal coefficient dataset, C_{X_S} : (a) $\phi' = 0$ deg; (b) $\phi' = 15$ deg; (c) $\phi' = 30$ deg; (d) $\phi' = 45$ deg; (e) $\phi' = 90$ deg.	177
A.2	CFD static lateral coefficient dataset, C_{Y_S} : (a) $\phi' = 0$ deg; (b) $\phi' = 15$ deg; (c) $\phi' = 30$ deg; (d) $\phi' = 45$ deg; (e) $\phi' = 90$ deg.	178
A.3	CFD static vertical coefficient dataset, C_{Z_S} : (a) $\phi' = 0$ deg; (b) $\phi' = 15$ deg; (c) $\phi' = 30$ deg; (d) $\phi' = 45$ deg; (e) $\phi' = 90$ deg.	178
A.4	CFD static rolling coefficient dataset, C_{l_S} : (a) $\phi' = 0$ deg; (b) $\phi' = 15$ deg; (c) $\phi' = 30$ deg; (d) $\phi' = 45$ deg; (e) $\phi' = 90$ deg.	179
A.5	CFD static pitching coefficient dataset, C_{m_S} : (a) $\phi' = 0$ deg; (b) $\phi' = 15$ deg; (c) $\phi' = 30$ deg; (d) $\phi' = 45$ deg; (e) $\phi' = 90$ deg.	179
A.6	CFD static yawing coefficient dataset, C_{n_S} : (a) $\phi' = 0$ deg; (b) $\phi' = 15$ deg; (c) $\phi' = 30$ deg; (d) $\phi' = 45$ deg; (e) $\phi' = 90$ deg.	180
A.7	C_{X_S} interpolation NRMSE comparison at different flight conditions: (a) $\phi' = 0$ deg; (b) $\phi' = 15$ deg; (c) $\phi' = 30$ deg; (d) $\phi' = 45$ deg; (e) $\phi' = 90$ deg.	184
A.8	C_{Y_S} interpolation NRMSE comparison at different flight conditions: (a) $\phi' = 15$ deg; (b) $\phi' = 30$ deg; (c) $\phi' = 45$ deg; (d) $\phi' = 90$ deg.	184
A.9	C_{Z_S} interpolation NRMSE comparison at different flight conditions: (a) $\phi' = 0$ deg; (b) $\phi' = 15$ deg; (c) $\phi' = 30$ deg; (d) $\phi' = 45$ deg.	185
A.10	C_{m_S} interpolation NRMSE comparison at different flight conditions: (a) $\phi' = 0$ deg; (b) $\phi' = 15$ deg; (c) $\phi' = 30$ deg; (d) $\phi' = 45$ deg.	185
A.11	C_{n_S} interpolation NRMSE comparison at different flight conditions: (a) $\phi' = 15$ deg; (b) $\phi' = 30$ deg; (c) $\phi' = 45$ deg; (d) $\phi' = 90$ deg.	186

List of Tables

1.1	Static coefficients CFD acquisition ranges.	34
1.2	Control coefficients CFD acquisition ranges.	38
2.1	Trim point conditions.	83
2.2	Model matching NRMSE evaluation.	85
2.3	NRMSE of the functions approximation.	90
3.1	Optimization analyses conditions.	128
3.2	Basis functions sets: AoA.	129
3.3	Basis functions sets: airspeed.	129
3.4	Basis functions sets: altitude.	129
4.1	Input DKM results.	149
4.2	‘Multi-loop’ output DKM results.	149
4.3	‘Loop-at-a-time’ output DKM results.	149
4.4	Sets of relative uncertainty levels.	153
4.5	Set of initial elevation angles.	156
4.6	Wind turbulence parameters.	161
4.7	Wind gusts parameters.	161
4.8	Controller interpolation functions analysis.	166

Table of Acronyms

AoA	<i>Angle-of-Attack</i>
AoS	<i>Angle-of-Sideslip</i>
BTT	<i>Bank-To-Turn</i>
CCF	<i>Course-Corrected Fuze</i>
CFD	<i>Computational Fluid Dynamics</i>
CL	<i>Closed-Loop system</i>
CM	<i>Center of Mass</i>
CP	<i>Center of Pressure</i>
DCM	<i>Direction Cosine Matrix</i>
DKM	<i>Disk Margin</i>
DoF	<i>Degrees-of-Freedom</i>
GM	<i>Gain Margin</i>
GNC	<i>Guidance, Navigation & Control</i>
GPS	<i>Global Positioning System</i>
GR	<i>Grid-Based</i>
INS	<i>Inertial Navigation System</i>
ISA	<i>International Standard Atmosphere</i>
IMU	<i>Inertial Measurement Unit</i>
LDR	<i>Lift-to-Drag Ratio</i>
LF	<i>Load Factor</i>
LFT	<i>Linear Fractional Transformation</i>
LMI	<i>Linear Matrix Inequality</i>
LPV	<i>Linear Parameter-Varying</i>
LR	<i>Linear Regression</i>
LRGP	<i>Long Range Guided Projectiles</i>

LTI	<i>Linear Time-Invariant</i>
MIMO	<i>Multiple Inputs Multiple Outputs</i>
MM	<i>Modulus Margin</i>
MoI	<i>Moment of Inertia</i>
MPC	<i>Model Predictive Control</i>
MR	<i>Multivariable Regression</i>
NDI	<i>Nonlinear Dynamic Inversion</i>
NED	<i>North-East-Down</i>
NL	<i>Nonlinear Systems</i>
NP	<i>Nominal Performance</i>
NRMSE	<i>Normalized Root Mean Square Error</i>
NS	<i>Nominal Stability</i>
PGK	<i>Precision Guidance Kit</i>
PGM	<i>Precision Guided Munition</i>
PM	<i>Phase Margin</i>
PR	<i>Polynomial Regression</i>
PY	<i>Polytopic</i>
quasi-LPV	<i>quasi-Linear Parameter-Varying</i>
RMSE	<i>Root Mean Square Error</i>
RP	<i>Robust Performance</i>
RS	<i>Robust Stability</i>
SDP	<i>Semi-Definite Programming</i>
SISO	<i>Single Input Single Output</i>
SOCBT	<i>Secant Ogive Cylinder Boat Tail</i>
TA	<i>Taylor Approximation</i>
s.t.	<i>such that</i>
w.r.t.	<i>with respect to</i>

Nomenclature

General Notation

x	Scalar value
\boldsymbol{x}	Vector
X	Matrix
\boldsymbol{x}^T (or X^T)	Transpose of \boldsymbol{x} (or X)
\boldsymbol{x}^{-1} (or X^{-1})	Inverse of \boldsymbol{x} (or X)

Tensor Algebra Notation

\boldsymbol{x}	Vector (tensor form)
\boldsymbol{X}	Matrix (tensor form)
$[\star]^B$	Projection w.r.t. the coordinate system B

Control Notation

\mathbb{R}	Real values set
\mathbb{C}	Complex values set
X^T	Transpose of $X \in \mathbb{R}$
X^*	Conjugate of $X \in \mathbb{C}$
$X \succ (\succeq) 0$	Symmetric and positive (semi)definite matrix
$X \prec (\preceq) 0$	Symmetric and negative (semi)definite matrix
$(\star)^T$	Conjugate (or transpose) element of a matrix $\in \mathbb{C}$ ($\in \mathbb{R}$)
$\text{Co}(\Gamma)$	Convex hull of the set Γ
$\mathcal{A}, \mathcal{B}, \mathcal{C}, \mathcal{D}$	System state space matrices
$\mathcal{F}_l(\star, \star)$	Lower linear fractional transformation
$\mathcal{F}_u(\star, \star)$	Upper linear fractional transformation
$\bar{\sigma}(X)$	Maximum singular value of X

Introduction

Contextualization

The Advent of Guided Missiles Technologies

The development of sophisticated missiles (ballistic and cruise) and artillery munitions technologies has represented a statement of power since their early design. Ballistic missiles are generally rocket-propelled only in the initial ascending phase of their trajectory (boost), between the launch to the apogee stage. They can be considered a range and power extensions of standard cannon-launch artillery munitions in reason of the larger dimensions and the capability to deliver different payload (explosive, nuclear, chemical, and biological warhead). Cruise missiles are powered by air-breathing jet engines along the entire flight, and are characterized by a lower regime (subsonic or transonic) atmospheric flight, relying on aerodynamic lift for trajectory flight control.

With the beginning of World War II, a significant effort has been dedicated to the enhancement of missiles' accuracy and range performance. The first employment of jet-propelled missiles, such as the German Vergeltungswaffen-1 (V-1 cruise missile) ([Gil44]; [Zal11]) and Vergeltungswaffen-2 (V-2 ballistic missile) ([Dor63]; [Zal13]) in 1944–1945, with an operating range of about 300 km, initiated a new rush for the technological supremacy among the most influential nations, leading to the development of the Sovietic R-1 SS-1 *Scunner* (300 km range) in 1958, and the first multistage intercontinental ballistic missile (ICBM) R-7 *Semyorka* (8000 km range) in 1957 ([Afa98]). As a response, between 1959 and 1965, the US short-range ballistic missile (SRBM) MGM-52 *Lance* ([Gro17]), the medium-range ballistic missile (MRBM) PGM-19 *Jupiter*, and the intermediate-range ballistic missile (IRBM) PGM-17 *Thor* ([CA91]) became operational, followed by the series of ICBM missiles SM-65 *Atlas* D-E and F (12000 km range) ([Sor60]; [Genb]; [Gena]), and the SM-68 *Titan* I-II (10000 km range) ([Stu00]). Meanwhile, similar short-range weapons were tested in France (AMX 30 *Pluton* missile ([Gal76])), in the Soviet Union (SS-21 *Scarab* [PS90]), and China (SRBM SS-2, MRBM CSS-1, IRBM CSS-2, and ICBM CSS-4 *Dong Feng* series ([Pra89])).

During the Cold War, range capability represented a core deterrent of power balance, resulting in the design of increasingly sophisticated weapons, such as the series of ICBM LGM-30 *Minuteman* I, II, III between 1962-1975 ([MC65]; [Hee12]), providing a maximum operating range of 13000 km, and equipped with an inertial navigation system (INS). The limited accuracy of early guidance technologies was soon balanced through the deployment of large-scale warheads (weapons of mass destruction (WMD)), ensuring the accomplishment of extremely long-range missions. The intensification of global tension around WMD employment lead to the establishment in 1987 of the Missile Technology Control Regime (MTCR) ([Ozg94]), with the core intention of limiting the proliferation of missile technologies, especially towards nuclear weapons development. The negotiations between the US and the Soviet

Union, officially referred to as the Strategic Arms Limitation Talks (SALT I-II) ([Sma70]) held between 1969-1979, culminated in the Intermediate-Range Nuclear Forces Treaty (INF) of 1987 ([Kno93]), with the intent to limit the employment of nuclear warheads. Between 1991-1997 the Strategic Arms Reduction Treaty START I-II-III ([OPB96]) began the process of nuclear demilitarization, finalized with the Strategic Offensive Reductions Treaty (SORT) of 2002 ([WFAT03]). These international agreements have been later renovated in 2010 with the New Strategic Arms Reduction Treaty (New START), stipulated between the Russian Federation and the US. However, the interest of the most influential nations to maintain a dominant role in geopolitical warfare often resulted in the refusal of treaties concerning the limitation of weapons range and power capability. Recently in 2023, with the begin of the war between Russia and Ukraine, Russia declared the suspension of its participation in the New START ([Bug23]).

The limitation imposed by the international treaties encouraged focusing the attention on the development of shorter-range tactical missile programs. Additionally, the accuracy and precision enhancements guarantee higher on-target effectiveness in military offensive and interception missions, and consequentially significantly lower operating costs. The advent of more advanced guidance technologies boosted the employment of ballistic missiles and cannon-launched artillery munitions as conventional weapons. Early trajectory-tracking guidance strategies were accomplished through radar or optical measurements from the launch site, while radio or laser control commands were transmitted by a ground operator. Guidance accuracy improved through the employment of television cameras and laser beams for target interception. In the 1950s, INSs began to be installed on long-range ballistic missiles, and later on tactical artillery-guided munitions in the 1970s, through the development of more advanced and cheaper electronic components.

Inertial navigation relies on the employment of accurate gyroscope and accelerometer measurements to estimate the position, heading, and velocity of missiles along their trajectory. The absence of electronic emissions in INSs represented a core advantage compared to alternative technologies, being more difficult to be identified. In 1986 the *Minuteman* IIIs were replaced by the more advanced US MX *Peacekeeper* missile ([Mac87]), equipped with INSs and an exterior celestial navigation system that used the stars or satellites as a reference to estimate the missile's position. The TERrain COntour Matching navigation technique (TERCOM) ([Gol80]) was later employed on the submarine-launched cruise missile (SLCM) *Tomahawk* and on its ground-launched versions (GLCM), the BGM-109G *Gryphon* ([Kop05]), where trajectory corrections were evaluated by means of digitalized contour maps obtained from radar measurements. Modern navigation systems incorporate advanced Global Navigation Satellite Systems (GNSSs) tracking technologies as the Global Positioning System (GPS), or the Global Navigation Satellite Systems (GLONASS), to complement the performance of standard INSs. Infrared seekers, radar, and optical gyroscopes generally provide more precise information during on-target fast-homing maneuvers.

The Development of Precision Guided Munition

The first examples of precision guided munition (PGM) or ‘smart munition’ can be traced during World War II in the German radio-controlled gliding bomb Ruhrstahl SD1400X (*Fritz X*) ([PP97]), employed in parallel with the V-1 and V-2 missiles by the Luftwaffe to hit enemy battleships. The proven effectiveness in the battlefield, in contrast with the standard unguided weapons, encouraged the broadening of PGMs to more versatile ground launchers as tank, mortar, and howitzer (such as the U.S. M109A6/A7 *Paladin* and the French Camion Équipé d’un Système d’Artillerie (CAESAR)). In addition, the constraints imposed in the 1970s with the SALT I, and advances in microprocessors and microelectronics development increased the interest in cannon-launched ammunition characterized by appealing lower production costs and increasingly higher performance in terms of accuracy and operating range. Differently from most of the long-range ballistic missiles, guided munition trajectories lie in the lower atmosphere and rely on aerodynamic lift-based corrections imposed through the employment of aerodynamic surfaces (tail-fins/rudders, nose-mounted canards, wings-flaps, and elevators) ([CA00]; [DM08]; [SC10]; [Fre11]; [CFC12]). This solution provides with higher control authority for the autopilot design, as well as a continuous-time trajectory correction [Wr98] compared to more complicated systems relying on thrust vectoring ([JC01]; [GC02]; [BPC02]; [CWB11]), or inertial effectors ([Mur78]; [HJ89]; [FC06]; [RC08]).

The airframe stability of aerodynamic-controlled ballistic munitions is generally addressed at the design stage by selecting among two main approaches: spin-stabilization or fin-stabilization. The former architecture takes advantage of the aerodynamic forces and moments generated by the high spin rate characterizing the body roll axis, which is transmitted to the projectile at the firing stage. A relevant advantage of spin-stabilized technologies relies on the possibility of retrofitting existing unguided munitions with course-corrected fuzes (CCFs) to implement guidance and control strategies. Successful applications correspond to the U.S. ATK’s M1156 Precision Guidance Kit (PGK) ([PBC07]; [Sto08]), the French Système à Précision Améliorée par Cinémomètre Doppler (SPACIDO) ([Cam07]), the U.K. Smart Trajectory Artillery Round (STAR) ([GL08]; [GL09]), and the European Correction Fuze (ECF) ([Per11]). In the last decades, relevant research contributions have been carried out also at the French-German Research Institute of Saint-Louis (ISL) through the studies of Course Correction Fuze (CCFus project) projectile systems ([TW11]; [TMW11]; [TSW15]; [Sev+17]; [Tha+19]; [Tip+20]; [Pin+22]). Nevertheless, the spin-stabilized architecture presents significant drawbacks deriving from the high spin rate characterizing the projectile. Indeed, the spin generates undesired nonlinear couplings between the normal and the lateral axes dynamics ([LB79]), which can represent a non trivial challenge to face during the flight control design. Additionally, spin-stabilized projectiles generally suffer from a limited operating range, depending on the capability of the firing gun and the firing conditions.

The aerodynamics of fin-stabilized munitions is closer to standard ballistic missiles, where the employment of a non-spinning concept reduces the highly nonlinear dynamics generated by the aerodynamic coupling terms, simplifying the general flight dynamics modeling stage. However, it requires specific tail-fins configurations for stability augmentation, which can increase the design and development expenses. Several applications have been already proposed by

different countries, such as the U.S. laser-guided artillery round M712 *Copperhead* ([MA77]; [NPM79]), the more recent 155 mm GPS-guided munition M982 *Excalibur* ([Wel00]), the XM395 Precision Guided Mortar Munition (PGMM) ([Mal+08]), the Italo-German long-range GPS/IR guided munitions *Vulcano* (B-C), the French semi-active laser guidance kit under the Metric Precision artillery Ammunition demonstrator (MPM) program, and the Russians 120 mm guided mortar weapon system KM-8 *GRAN* and laser-guided projectile 30F39 *Krasnopol* ([Gra05]). The autopilot design of fin-stabilized munitions can be generally performed separately for each single axis ([Bla91]), and the projectile aerodynamics is generally less affected by large and rapid variations of the flight parameters.

The continuous development in guided munitions technologies observed in the past decades has been boosting the research competition between the most influential countries worldwide. The further enhancement of the range and accuracy performance, under the minimization of the development design costs (e.g. the avoidance of any modifications of the existing firing guns), implies the investigation of innovative aerodynamic configurations and flight control strategies. A promising solution could be identified in a novel fin-stabilized architecture with a reduced number of control actuators, investigated at ISL, aiming to ameliorate the range capability through a gliding steered flight. Early studies have revealed the advantages provided by fin-stabilized design compared to spin-stabilized systems ([Cha+17]), suggesting the employment of glider-like projectile configurations in combination with Bank-To-Turn (BTT) flight strategies. Interesting properties of the analyzed concept derive from selecting a reduced set of control actuators, leading to an asymmetric canards/fins configuration ([Fre11]; [CFC12]) and a predominant statically unstable behavior. Additionally, recent research on long-range guided projectiles ([Vas+20]) underlined the impact of the canards/fins configuration, aerodynamics modeling, and guidance development on the overall range capability.

Guided Munitions Design

The Guidance, Navigation & Control Design Loop

The design of guided weapons consists of the definitions and cooperation of three different functionality: Guidance, Navigation & Control (GNC). The standard GNC double-loop implementation is represented in Figure 1. A faster inner loop updates the control commands evaluated by the autopilot based on the information provided by the navigation algorithm, while a slower outer loop updates the reference signals generated by the guidance law to accomplish the requirements of the mission.

Guidance. Consists of optimization algorithms that determine the reference signals that have to be followed by the vehicle to accomplish a predefined objective, depending on the selected mission. The guidance law relies on the information provided by the navigation system in terms of available measurements or estimated parameters, determining the current state of the vehicle. Guidance systems differ generally by the technology they rely on and

the type of target they aim to. Classical approaches implement onboard guidance computers (called ‘homing’ guidance) to hit moving targets through proportional navigation principles ([Gue71]; [KPT13]), or active/passive homing systems employing radar and infrared seekers ([Wal02]; [VM82]). When aiming at a fixed target, no trackers are generally required and the information on the target positions is known a priori. In this scenario, navigational guidance systems provide a continuous self-evaluation and correction of the vehicle trajectory based on the known location of the target. Typical examples are the aforementioned inertial guidance (employing gyroscopes and accelerometers) ([Bra+13]), astro-inertial guidance (based on celestial navigation [AZF06]), and terrestrial guidance (as the TERCOM [Gol80]). Additionally, guidance laws can be categorized w.r.t. the specific phase of the trajectory they are engaged for (mid-course guidance, terminal guidance), characterized by different objectives (e.g. range optimization, target interception) and reference signals (e.g. accelerations, body rates).

Navigation. Implements sophisticated algorithms for an accurate estimation of the current state of the vehicle in time (in terms of position, heading, velocity). Navigation systems rely on the available sensors’ measurements relative to fixed/relative reference targets or track the relative position from a priori known point. Additionally, advanced algorithms are generally developed to estimate unmeasured information, based on sensor data fusion (as in Kalman filters [Her17]). A typical technology embedded in ballistic missiles consists of inertial measurement units (IMUs) allowing for inertial dead-reckoning navigation strategies, where the position is estimated through inertial acceleration measurements ([OFS98]; [Tit+04]). More advanced navigation systems employ GNSS, radar, and infrared measurements, depending on the operational requirements of the vehicle ([Ohl+97]; [Qua+15]). Sensor data fusion algorithms represent a common strategy often used also to correct individual measurements from external noise sources.

Control. The control design accounts for the current state information provided by the navigation systems to determine the optimal control actions to be set on the available actuators thus to implement the desired guidance strategy. In early guided systems, the control actions were performed by ground operators at the launch site, and transmitted to the vehicle by means

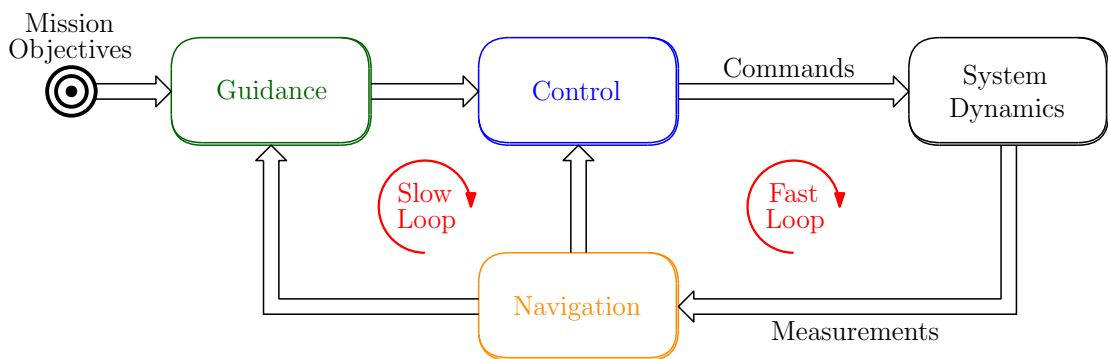


Figure 1: Guidance, Navigation, and Control (GNC) double-loop design.

of radar or laser signals. With the advent of electronic embedded systems, onboard autopilots have been designed to implement completely autonomous or semi-autonomous guided vehicles. The autopilot design relies on the development of dedicated control-oriented models of the system dynamics, characterizing the stability and performance of the system. The amount and the type of actuators installed on the system, determine the allocation strategy (static or dynamic) selected to implement the control command. This aspect strongly affects the capability of the system to perform certain maneuvers (control authority), and consequently the overall optimal control law design.

Autopilot Design Approaches: the Gain-Scheduling Control Strategy

Concerning aerospace applications, modeling and control design has always represented a tedious process to be accomplished. The high non-linearity characterizing vehicles' flight dynamics and the large variety of operational parameters to account for increase significantly the complexity of the design. Thus, an exhaustive analysis of the behavior of the system under investigation is required. Indeed, the derivation of an effective control law strongly relies on the accuracy of the model selected to represent the system dynamics. Nonetheless, the complexity of the control-oriented model affects the selection of the most appropriate control approach and eventually the numerical burden of the controller implementation. Thus, a proper trade-off between complexity and accuracy needs to be achieved. Furthermore, dealing with missile and projectile technologies implies a generally limited availability of control effectors (and related authority), combined with a larger variation of the flight parameters characterizing the typical ballistic trajectory, exploding the complexity of the overall design process.

Aiming to withstand a wide set of flight conditions, the operating domain of ballistic missiles and projectiles is composed of a selected set of parameters such as Mach number, \mathcal{M} , altitude, h , and angle-of-attack (AoA), among others. The resulting subspace of the flight envelope is represented as a grid of targeted operating points, as shown in Figure 2(a). Several control design approaches can be employed for autopilot synthesis at the targeted conditions. Nonlinear techniques based on feedback linearization gained popularity in the last decades in reason of the possibility to directly account for the nonlinearities of the system dynamics. Nonlinear dynamic inversion (NDI) methods have been successfully used on a wide range of missile and projectile applications ([Tip+20]; [Pin+22]; [Pin+23]; [Pfi12]) in combination with adaptive and robust approaches, depending on the addressed scenario. However, the linear time-invariant (LTI) framework still provides a broader range of design techniques and analysis tools, thanks to the intrinsic properties characterizing linear system theory. In order to exploit these properties, the nonlinear dynamics of flying vehicles is commonly linearized at targeted flight conditions (series expansion linearization), resulting in a collection of local linear representations of the original model. This method allows for employing linear control design techniques for autopilot synthesis.

In this context, a well-established strategy consists of decomposing the overall control task into the design of local LTI controllers at each local linearization of the original nonlinear dynamics. The resulting set of local LTI controllers can be easily implemented through the

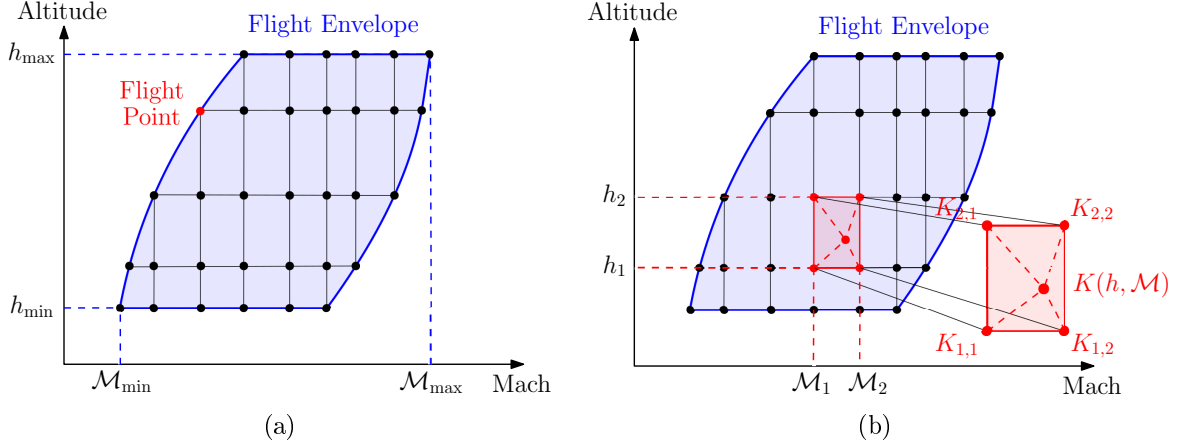


Figure 2: Gain-scheduling: (a) flight envelope parametrization; (b) controller, K , linear interpolation.

definition of a dedicated scheduling strategy, which allows selecting the most appropriate controller at any operating condition. The most traditional scheduling strategy relies on the linear interpolation of the local controllers' static gains, referred to as the gain-scheduling approach. As shown in Figure 2(b), depending on the flight parameters designated as scheduling variables, a controller, K , is obtained at any flight conditions in the operating envelope as the linear interpolation between the designed set of local LTI controllers ([HG93]; [NRR93]). A relevant advantage related to this strategy consists of the possibility of employing any control technique for the design of the local controllers. First developed in the 1960s the gain-scheduled control became a popular strategy in the 1990s ([SA90]; [Rug90]; [LL00]; [RS00]), leading to successful applications in the aerospace environment. Concerning the military sector, early examples of gain-scheduling design can be traced in the Nike Ajax missile, where the gain of the fin control system and roll autopilot were scheduled via dynamic pressure measurements, or the Talos missile ([Pad82]), implementing an altitude-based gain-scheduling system.

In the last decades, several missile/projectile technologies have relied on the gain-scheduling strategy, in reason of its high versatility to be complemented with advanced design approaches and implementation ease. Interesting \mathcal{H}_∞ -based applications can be found in [LSZ14]; [LSZ16], and in [BGL22]; [GB22]; [GA13] where alternative tuning approaches are proposed to optimize the control design process. Significant contributions have been investigated also at ISL through the development of gain-scheduled strategies for robust \mathcal{H}_∞ autopilot design ([TD09]; [TSW15]; [TP21]; [Str+18]; [ST19]), loop-shaping techniques ([Sèv+14]; [Sè+17]), and anti-windup strategies ([Tha+20]; [Tha+23]).

Thesis Motivations

Despite a broad range of successful applications, gain-scheduling design has been proven to present important theoretical and practical limitations, which are discussed in the following:

- I. Accuracy.** From the modeling perspective, standard linearization-based gain-scheduling design is performed on a collection of LTI local linearizations of the original nonlinear system dynamics, at selected operating conditions (equilibrium points or trajectories). As a consequence, the linearized models provide only locally reliable representations of the nonlinear system, leading to the possible loss of important information regarding the system's transient behavior. Alternative approaches, implementing a velocity-based linearization, attempted to partially preserve the dynamic properties of the nonlinear system ([LL98]).
- II. Stability.** Concerning the control design, several approaches can be employed for the synthesis of local controllers based on the set of LTI linearizations of the system dynamics. However, in reason of the local validity of the LTI models, the obtained controllers ensure only local closed-loop stability guarantees in the vicinity of the selected flight points. Thus, no a priori guarantees about the stability and the performance of the local controllers' interpolation are provided at generic flight conditions across the envelope. Typical solutions to this problem rely on frozen-time theory, where the variation of the scheduling parameters across the equilibrium points is assumed 'slow enough' such that local stability properties are preserved ([KK91]; [LR90]). However, the slow-variation assumption can be extremely conservative for many application scenarios, since the guaranteed stability properties correspond to the worst-case robustness of the overall collection of LTI local systems ([SA90]; [SA92]).

In the aerospace sector, a widespread design solution consists of extending the linearization on a dense grid of conditions, and a posteriori, testing the controller robustness on a much denser grid. Nevertheless, this process requires time and high computational power since it generates a large number of local controllers to be implemented for the interpolation.

In the last decades, the linear parameter-varying (LPV) framework has attracted increasing interest in the modeling and control of a wide range of aerospace applications. Early studies in the 1990s proposed the LPV modeling approach as a perfect match for the gain-scheduling control design technique, leading to relevant contributions concerning missile ([SC93]; [CS96]; [PPV01]; [TPB00]) and aircraft ([Bal+97]; [YWA13]; [HSB14]) applications. Differently from linearization-based approaches, the LPV gain-scheduling design directly targets the synthesis of the overall controller, providing closed-loop stability properties in a global sense. Furthermore, LPV/quasi-LPV models can account for the time variations of a selected set of parameters, which results into a higher capability in capturing the nonlinear system dynamics ([MB04]; [PH11]; [PVR12]). The LPV controller synthesis is achieved through the resolution of an optimization problem formulated as a set of linear matrix inequalities (LMIs). The problem formulation can be accomplished either by exploiting the features of parameter-affine

systems, or by discretizing the parameters space by means of a gridding process. The former solution (polytopic) provides higher guarantee of quadratic stability of the closed-loop system, at the expenses of more conservative performance ([ABG95]; [AGB95]). The latter (grid-based) stands as a natural extension of the standard gain-scheduling design to the LPV framework, providing significant performance together with higher implementation complexity and lower global stability properties ([WPB95]; [Wu+96]).

Several studies have also focused on the investigation of guided projectile technologies. LPV modeling has been coupled with \mathcal{H}_∞ robust control design for spin-stabilized ([S  v+14]; [The+13]; [TSW15]; [The+10]), and fin-stabilized ([Str+18]; [ST19]) projectiles' architectures. However, the LPV models were generally obtained as a family of local linearizations of the original nonlinear dynamics, while the control strategy relied on standard gain-scheduling autopilot interpolations. Only recently, an LPV approach has been developed in the framework of model predictive control (MPC) ([BG22]). The proven advantages characterizing the LPV class of systems, in contrast with the still limited amount of applications concerning guided munitions design, open several opportunities for further investigations. Additionally, the development of more sophisticated algorithms and more powerful tools for the resolution of complex LMIs optimization problems allows the design of controllers of increasing performance.

The above introduction consists of a non-exhaustive overview of the state-of-the-art concerning aerospace control technologies and LPV design applications. A dedicated discussion is provided in the introduction of each chapter of the manuscript.

LRGP Project and Thesis Objectives

The proposed thesis is part of the Long Range Guided Projectile (LRGP) *contract de subvention (CS)* begun in 2018 as a collaboration between the Direction G  n  rale de l'Armement (DGA) and the French-German Research Institute of Saint-Louis ([Mar+18]; [Lib+19]; [Lib+20]; [Lib+21]). The core intent of the LRGP project relies on the range enhancement of standard low-cost 155 mm artillery projectiles, accounting for the minimization of the necessary time of flight. In this context, the thesis focuses on the projectile flight dynamics modeling and the LPV-based autopilot design, employed during the guided phase of the projectile trajectory to track a range extension guidance law. The main objectives of the thesis can be summarized as follows:

- ❖ Flight dynamics modeling of the new LRGP concept, including a complete aerodynamic characterization of the projectile.
- ❖ Development of a 6-DoF nonlinear simulator environment to test the performance of the projectile in multiple operating flight scenarios.
- ❖ Derivation of the LPV-based control-oriented model design of the projectile nonlinear dynamics without employing local linearization-based techniques.

- ❖ Investigation of different LPV-based robust controller design approaches for the development of a gliding phase autopilot, providing stronger guarantees of stability and performance compared to standard LTI gain-scheduling techniques.
- ❖ Implementation of a range extension guidance law based on a BTT flight strategy to improve the operating performance of the projectile.
- ❖ Assessment of the performance and the robustness of the designed autopilot in the nonlinear simulator through realistic operating scenarios.

Thesis Contributions

The project investigates the complete characterization of a new concept of guided projectiles studied at the Institute of Saint-Louis, addressing both the modeling and the control design stages. Particular focus is dedicated in the linking process among the two design stages, where the requirements of various autopilot design approaches are targeted from the system modeling perspective. The main contributions achieved during the development of the project can be summarized in the following categories:

LPV-based Flight Dynamics Modeling Contribution

- I. LRGP flight dynamics and aerodynamics modeling.** The flight dynamics model of a new concept of long range guided projectile was derived starting from the standard aerospace theoretical formulation, and implemented in a complete simulator environment. In particular, the full characterization of the projectile's aerodynamics has resulted in the proposition of a novel ad-hoc designed aerodynamic model which accurately represents the projectile's behavior across a large envelope of flight conditions.

The complete formulation of the projectile nonlinear dynamics, including a dedicated section concerning the aerodynamics analysis and modeling process, is presented in Chapter 1.

- II. LPV modeling process of nonlinear flight dynamics.** A relevant aspect exhaustively discussed during the project consists of the non-trivial process of reformulation of the highly nonlinear projectile dynamics model as an accurate LPV system. Depending on the selected approach, multiple LPV models can be obtained from the same nonlinear system, exploiting different properties and features. Thus, a careful selection of the most appropriate varying parameters to be accounted for requires an accurate analysis of the system's behavior combined with the prior definition of the control design objectives.

The LPV modeling design of the projectile nonlinear dynamics is discussed in Chapter 2, where the employment of the state transformation approach allows deriving a reliable LPV model of the projectile pitch channel dynamics.

LPV-based Flight Control Design Contribution

III. Polytopic LPV \mathcal{H}_∞ control design for guided projectiles. The polytopic approach represents a well established LPV control design technique that has been employed for various applications to overcome the limitations of the standard LTI gain-scheduling design strategy. In the aerospace environment it has shown successful results in the autopilot synthesis for several applications. However, few investigations have dealt so far with trajectory tracking scenario of guided projectiles, covering a large range of flight conditions. Indeed, the conservativeness characterizing the polytopic formulation requires an accurate modeling and control design to ensure stability and satisfactory performance across the entire flight envelope targeted in the polytope definition.

The polytopic model analysis and formulation is presented in details in Chapter 2, while Chapter 3 discusses the corresponding autopilot design and robustness properties. Additionally, a robustness analysis and trajectory tracking simulations are proposed in Chapter 4 to assess the performance of the controller in the nonlinear simulator environment.

IV. Uneven grid-based LPV \mathcal{H}_∞ control design for guided projectiles. LPV grid-based design consists of a more recent alternative solution for controller synthesis. It allows relaxing the conservativeness affecting the standard polytopic approach by gridding the parameter space. In particular, it ensures stability properties through the identification of a set of parameter-dependent Lyapunov functions. However, the dimensions of the grid represent a critical aspect concerning the computational complexity of the controller synthesis. Thus, an accurate analysis of the flight envelope is required to properly select the operating conditions to be accounted for during the control design.

In Chapter 3, a modeling procedure is developed to analyze the properties of the projectile dynamics across the gridded parameters space to reduce the complexity of the autopilot synthesis. The assessment of the controller robustness and performance is presented in Chapter 4, through the implementation of multiple simulation scenarios in the nonlinear simulator environment.

Manuscript Outline

The proposed manuscript is organized into two core parts:

- ❖ Part I: is dedicated to the complete modeling procedure of the projectile dynamics, from the nonlinear flight dynamics derivation to the control-oriented LPV model design.
 - Chapter 1: concerns the formulation of the nonlinear dynamics of a new class of guided projectiles (LRGP). A detailed aerodynamic characterization allows the derivation of a dedicated aerodynamic model for the new projectile concept. The modeling procedure is finalized through the development of a complete simulator environment.
 - Chapter 2: provides a general introduction to the LPV class of systems, including a brief overview related to the LPV modeling approaches. The nonlinear dynamics of the projectile is then converted into an accurate LPV system. The final control-oriented modeling step consists of the reformulation of the projectile LPV model as a polytopic parameter dependent system.
- ❖ Part II: deals with the LPV-based autopilot design of the guided projectile, through the comparison of two main approaches, and their final performance validation.
 - Chapter 3: details the control design based on two distinct LPV-based techniques: polytopic and grid-based. A general overview recalls the fundamental concepts concerning the LPV controller synthesis processes through the formulation of LMIs based optimization problems. For each design approach, the controller synthesis performance are improved by means of dedicated analyses that target the optimization of the related computational complexity.
 - Chapter 4: is dedicated to the main simulation results, consisting of realistic trajectory tracking scenarios. The performances of the designed LPV controllers are evaluated in the complete simulator environment addressing various sources wind disturbances. Additionally, stability margins and μ -sensitivity analyses provide a preliminary evaluation of the controllers robustness properties.

A final chapter is dedicated to the concluding remarks on the achieved results, and the proposition of possible future developments.

List of Publications

Journal Papers

Title: Linear Parameter-Varying Polytopic Modeling and Control Design for Guided Projectiles.

Authors: Vinco, G.M., Sename, O., Strub, G. and Theodoulis, S.

Journal: AIAA Journal of Guidance, Control, and Dynamics.

Status: Published, **Year:** 2024, **Volume:** 47, **Number:** 3, **Pages:** 433-447.

International Conference Papers with Proceedings

Title: Flight Dynamics Modeling and Simulator Design for a New Class of Long-Range Guided Projectiles.

Authors: Vinco, G.M., Theodoulis, S., and Sename, O.

Conference: 6th CEAS Conference on Guidance, Navigation and Control (EuroGNC 2022).

Venue: Berlin, Germany; **Date:** May 3-5, 2022.

Title: Quasi-LPV Modeling of Guided Projectile Pitch Dynamics through State Transformation Technique.

Authors: Vinco, G.M., Theodoulis, S., Sename, O., and Strub, G.

Conference: 5th IFAC Workshop on Linear Parameter Varying Systems (LPVS 2022).

Venue: Montreal, Canada; **Date:** September 27-30, 2022.

Title: Linear Parameter Varying Pitch Autopilot Design for a class of Long Range Guided Projectiles.

Authors: Vinco, G.M., Theodoulis, S., Sename, O., and Strub, G.

Conference: 2023 AIAA Science and Technology Forum and Exposition (SciTech Forum).

Venue: National Harbor, Maryland, US; **Date:** January 23-27, 2023.

Title: Uneven Grid-based Linear Parameter-Varying Controller Design for Guided Projectiles.

Authors: Vinco, G.M., Theodoulis, S., Sename, O., and Strub, G.

Conference: 22nd World Congress of the International Federation of Automatic Control (IFAC World Congress 2023).

Venue: Yokohama, Japan; **Date:** July 9-14, 2023.

International Workshops without Proceedings

Title: Flight Dynamics Modeling for Long Range Guided Projectiles (LRGP).

Authors: Vinco, G.M., Theodoulis, S., and Sename, O.

Conference: Novelties in Guidance, Navigation and Control (e-EuroGNC 2021).

Venue: Online; **Date:** October 7, 2021.

National Conferences and Workshops without Proceedings

Title: Flight Dynamics Modeling for Long Range Guided Projectiles (LRGP).

Authors: Vinco, G.M., Theodoulis, S., Sename, O.

Conference: 10th Budding Science Colloquium at ISL

Venue: Saint-Louis, France; **Date:** September 27-28, 2021.

Title: Quasi-LPV Modeling and Control of Projectile Pitch Dynamics through State Transformation Technique.

Authors: Vinco, G.M., Sename, O., Theodoulis, S., and Strub, G.

Conference: Journées de printemps de la SAGIP 2022.

Venue: Bidart, France; **Date:** May 23-25, 2022.

Title: Uneven Grid-based Linear Parameter-Varying Controller Design for Guided Projectiles.

Authors: Vinco, G.M., Theodoulis, S., Sename, O., and Strub, G.

Conference: [CT CPNL] Premier congrès annuel de la SAGIP.

Venue: Marseille, France; **Date:** June 7-9, 2023.

Title: Grid-based Linear Parameter-Varying Controller Design for Guided Projectiles.

Authors: Vinco, G.M., Strub, G., and Sename, O.

Conference: 12th Budding Science Colloquium at ISL

Venue: Saint-Louis, France; **Date:** September 27-28, 2023.

Part I

Projectile Modeling Design: From the nonlinear to the LPV-based model formulation

Flight Dynamics Modeling

Contents

1.1	Introduction	17
1.2	Flight Mechanics	19
1.2.1	Tensor Algebra	19
1.2.2	Reference Frames and Coordinate Systems	22
1.2.3	6-DoF Projectile Equations of Motion	25
1.2.4	The LRGP Concept	29
1.3	Projectile Aerodynamic Characterization	32
1.3.1	Aerodynamics Formulation	32
1.3.2	Computational Fluid Dynamics Data	33
1.3.3	Aerodynamics Modeling	39
1.4	6-DoF Simulator Environment	52
1.4.1	The SMART Toolbox	52
1.4.2	Nonlinear Simulator	52
1.4.3	Model Validating Simulations	55
1.5	Concluding Remarks	57

1.1 Introduction

The modeling process of system dynamics represents the most crucial stage prior to the controller design. Indeed, a proper identification and description of the system behavior improves the reliability of the mathematical model and enhances the effectiveness of the controller. However, an excessively detailed model would explode the complexity of the controller design with the risk of diminishing the achievable performance or making it unfeasible for any practical implementation. As a consequence, a compromise between accuracy and complexity is generally required. A common practice consists of the derivation of simplified model dynamics dedicated to the controller design, capturing only the most relevant features that affect the targeted controller performance. A detailed and exhaustive model of the system dynamics is eventually employed to test the controller design in a more realistic simulation scenario.

This chapter provides an overview of the complete derivation of the model dynamics for the new class of Long Range Guided Projectiles (LRGP) investigated at the Institute of Saint-Louis (ISL) ([Mar+18]; [Lib+19]; [Lib+20]; [Lib+21]). The model includes a combination of measured physical properties (such as concept dimensions, shapes, mass, and inertia) and estimated parameters (aerodynamic coefficients). The first part of the chapter is dedicated to the general formulation of the projectile flight mechanics ([Zip14]), later applied to the LRGP concept. An overview of the LRGP project highlights the main objectives to be targeted and achieved through the system modeling and the following controller design. The second part of the chapter concerns the aerodynamic characterization of the projectile's concept. An exhaustive dataset of Computational Fluid Dynamic (CFD) simulations is acquired and then analyzed by employing selected regression models. The results are used to characterize the aerodynamic terms in the general flight mechanics model of the projectile. The final nonlinear model is implemented in a simulator environment meant to test the performance of the final controller design.

The chapter is structured in the following sections:

- S1.2: concerns the derivation of the projectile translational and attitude dynamics and kinematics, first expressed in the more general tensor formulation and then projected in the proper coordinate systems. A detailed introduction to the LRGP concept highlights the most relevant physical properties accounted for in the modeling process.
- S1.3: discusses the complementary aerodynamic characterization through the results of an exhaustive CFD analysis, leading to the derivation of two complete aerodynamic models of increasing complexity and accuracy. The results presented in this section have been published in [Vinb].
- S1.4: presents the design of the simulator environment later employed for simulation purposes, which additionally targets the dynamics of the air variables characterizing the surrounding atmosphere and affecting the projectile flight performance. The results presented in this section have been published in [Vinb].

1.2 Flight Mechanics

This section is dedicated to the derivation of the nonlinear flight mechanic model characterizing the projectile dynamics. Section 1.2.1 first recalls the fundamental principles of the tensor algebra employed for the formulation of the projectile equations of motion. The main reference frames and their associated coordinate systems are presented in Section 1.2.2, while Section 1.2.3 discusses the general derivation of the projectile nonlinear model dynamics. Finally, Section 1.2.4 introduces the fundamental features of the LRGP concept and how they characterize the general nonlinear model dynamics.

1.2.1 Tensor Algebra

The dynamics of any physical phenomena is intrinsically independent from the metric system employed to observe them. Accordingly, the derivation of the dynamic equations governing the behavior of a flying vehicle has to be expressed in a coordinate invariant form that can be adapted to any suitable metrics. This concept is formalized in the following distinction:

Definition 1.1 (Frame)

Physical entity constituted by a continuous set of a minimum of three noncollinear points having mutually time invariant distances in the 3D Euclidean space. The location and the orientation of a reference frames are defined by a base point, A , and a triad of orthonormal base vectors:

$$\mathbf{a}_1, \mathbf{a}_2, \mathbf{a}_3 \quad \text{with} \quad \mathbf{a}_i^T \mathbf{a}_j = \begin{cases} 0 & \text{for } i \neq j \\ 1 & \text{for } i = j \end{cases}; \quad i, j = 1, 2, 3.$$

Definition 1.2 (Coordinate System)

Ordered set of numbers (scalar coordinates, $]^A$) that associates a specific vector with the 3D Euclidean space, based on a orthogonal triple of directions ($1^A, 2^A, 3^A$). Specifically, a Cartesian coordinate system, is a a set of coordinates that satisfies the finite differences Cartesian metric:

$$\Delta s^2 = \sum_{i=1}^3 \Delta x_i^2$$

where Δs represents a finite distance in the 3D Euclidean space and Δx_i^2 are mutually orthogonal elements.

Since a coordinate system does not refer to a specific physical quantity, several coordinate systems can be associated to the same frame. In particular, for each frame a *preferred* system of coordinates can be identified, whose directions are aligned with the base vectors of the frame, such that:

$$[\mathbf{a}_1]^A = [1 \ 0 \ 0]; \quad [\mathbf{a}_2]^A = [0 \ 1 \ 0]; \quad [\mathbf{a}_3]^A = [0 \ 0 \ 1].$$

The space-time invariance characterizing different frames and their interaction can be exploited by employing the mathematical tensors notation. Indeed, tensors are algebraic objects used to describe physical entities whose content is intrinsically independent from the coordinate system from which they are observed, as well as coordinate transformations invariant.

Definition 1.3 (Cartesian Tensors)

A ordered set of triples, \mathbf{x} , is a Cartesian vector (first-order tensor) if for any pair of allowable Cartesian coordinate systems, $]^A,]^B$, the following transformation holds:

$$[\mathbf{x}]^B = [\mathbf{T}]^{BA} [\mathbf{x}]^A. \quad (1.1)$$

A ordered set of 9-tuples, \mathbf{X} , is a Cartesian tensor (second-order tensor) if for any pair of allowable Cartesian coordinate systems, $]^A,]^B$, the following transformation holds:

$$[\mathbf{X}]^B = [\mathbf{T}]^{BA} [\mathbf{X}]^A [\mathbf{T}]^{BA,T} \quad (1.2)$$

where $[\mathbf{T}]^{BA}$ is the associated Coordinate Transformation Matrix which maps the coordinates of a tensor from system $]^A$ to system $]^B$.

The relative location and orientation between any pair of different frames, A and B , are defined respectively as a displacement vector, \mathbf{s}_{BA} , between the base points of the two frames, and as a rotation tensor, \mathbf{R}^{BA} .

Definition 1.4 (Rotation Tensor)

Given two frames, A and B , with triad of basis vectors, $(\mathbf{a}_1, \mathbf{a}_2, \mathbf{a}_3)$ and $(\mathbf{b}_1, \mathbf{b}_2, \mathbf{b}_3)$ respectively, the mutual orientation of frame B w.r.t frame A is defined by the rotation tensor \mathbf{R}^{BA} through the transformation:

$$\mathbf{b}_i = \mathbf{R}^{BA} \mathbf{a}_i; \quad i = 1, 2, 3. \quad (1.3)$$

In particular, when coordinated in the preferred coordinate systems, $]^A$ and $]^B$ respectively, the following property holds:

$$[\mathbf{R}^{BA}]^A = [\mathbf{r}^{BA}]^B = [\mathbf{R}]^{BA,T}.$$

The expression of the relative linear and angular motions between different frames implies addressing the time dependence of the displacement vector, $\mathbf{s}_{BA}(t)$, and the rotation tensor, $\mathbf{R}^{BA}(t)$, respectively. Furthermore, the time rate of change of these two quantities defines the corresponding relative linear and angular velocity, \mathbf{v}_B^A and $\boldsymbol{\omega}^{BA}$ respectively. Under the conditions of invariant coordinate transformation expressed in Equations (1.1)-(1.2), the linear and the angular velocities inherit the properties of Cartesian tensors. Concerning the angular velocity, these conditions implies the definition of the rotational time derivative operator.

Definition 1.5 (Rotational Time Derivative)

Given a first-order tensor, \mathbf{x} , the rotational time derivative, $\mathcal{D}^A \mathbf{x}$, w.r.t. any arbitrary frame, A , and expressed in any allowable coordinate system, $]^B$, corresponds to:

$$[\mathcal{D}^A \mathbf{x}]^B = \left[\frac{d\mathbf{x}}{dt} \right]^B + [\mathbf{T}]^{BA} \left[\frac{d\mathbf{T}}{dt} \right]^{BA,T} [\mathbf{x}]^B. \quad (1.4)$$

Equivalently, given a second-order tensor, \mathbf{X} , the rotational time derivative, $\mathcal{D}^A \mathbf{X}$, w.r.t. any arbitrary frame, A , and expressed in any allowable coordinate system, $]^B$, corresponds to:

$$[\mathcal{D}^A \mathbf{X}]^B = \left[\frac{d\mathbf{X}}{dt} \right]^B + [\mathbf{T}]^{BA} \left[\frac{d\mathbf{T}}{dt} \right]^{BA,T} [\mathbf{X}]^B + [\mathbf{X}]^B \left[\frac{d\mathbf{T}}{dt} \right]^{BA} [\mathbf{T}]^{BA,T}. \quad (1.5)$$

In reason of the coordinate invariant transformations in Equations (1.4)-(1.5), $\mathcal{D}^A \mathbf{x}$ and $\mathcal{D}^A \mathbf{X}$ are also tensors of first and second-order, respectively.

Based on the above definitions, the linear velocity and linear acceleration tensors of any point B w.r.t. any point belonging to a frame A can be obtained respectively as the first and the second-order rotational time derivative of the corresponding displacement vector:

$$\mathbf{v}_B^A = \mathcal{D}^A \mathbf{s}_{BA}; \quad \mathbf{a}_B^A = \mathcal{D}^A \mathcal{D}^A \mathbf{s}_{BA} = \mathcal{D}^A \mathbf{v}_B^A. \quad (1.6)$$

Equivalently, the relative rotation of a vector $\mathbf{b}(t)$ in frame B w.r.t. its initial position at t_0 in frame A is expressed by the rotation tensor \mathbf{R}^{BA} as in Equation (1.3). According to Equation (1.6), the tangential velocity of the rotating vector is defined by the first-order rotational time derivative:

$$\begin{aligned} \mathbf{v}_B^A &= \mathcal{D}^A \mathbf{b}(t) \\ &= \mathcal{D}^A \mathbf{R}^{BA} \mathbf{b}(t_0) \\ &= \mathcal{D}^A \mathbf{R}^{BA} \mathbf{R}^{BA,T} \mathbf{b}(t) \\ &= \boldsymbol{\Omega}^{BA} \mathbf{b}(t) \end{aligned}$$

where, the angular velocity tensor of frame B w.r.t. frame A corresponds to:

$$\boldsymbol{\Omega}^{BA} = \mathcal{D}^A \mathbf{R}^{BA} \mathbf{R}^{BA,T}.$$

In particular, the angular velocity tensor, $\boldsymbol{\Omega}^{BA}$, is skew symmetric, thus for any coordinates systems, $]^C$, the following vector equivalence holds:

$$[\boldsymbol{\Omega}^{BA}]^C = \begin{bmatrix} 0 & -z & y \\ z & 0 & -x \\ -y & x & 0 \end{bmatrix} \iff [\boldsymbol{\omega}^{BA}]^C = \begin{bmatrix} x \\ y \\ z \end{bmatrix}.$$

The coordinate invariant formulation of the rotational time derivative is always expressed w.r.t. a selected reference frame. Thus, the last fundamental concept to be recalled concern the possibility to change the reference frame through the tensor formulation of the standard Euler transformation.

Theorem 1.1 (Generalized Euler Transformation)

Assuming any pair of arbitrary reference frames, A and B , and the corresponding angular velocity tensor, $\boldsymbol{\Omega}^{BA}$, then the following rotational time derivative transformation holds for any vector \mathbf{x} :

$$\mathcal{D}^A \mathbf{x} = \mathcal{D}^B \mathbf{x} + \boldsymbol{\Omega}^{BA} \mathbf{x}.$$

More detailed information concerning the properties and the proofs of the aforementioned Definitions 1.1-1.5 and Theorem 1.1 are provided in [Zip14].